Theses and Dissertations

12-14-2015

Applications of Attenuated Total Reflectance Fourier Transform Infrared Spectroscopy for Forensic Analysis

Zhenyu Lu
University of South Carolina - Columbia

APPLICATIONS OF ATTENUATED TOTAL REFLECTANCE FOURIER TRANSFORM
INFRARED SPECTROSCOPY FOR FORENSIC ANALYSIS

by

Zhenyu Lu

Bachelor of Science
Nanjing University, 2011

Submitted in Partial Fulfillment of the Requirements

For the Degree of Doctor of Philosophy in

Chemistry

College of Arts and Sciences

University of South Carolina

2015

Accepted by:

Stephen L. Morgan, Major Professor

S. Michael Angel, Committee Chair

Michael L. Myrick, Committee Member

Blaine D. Griffen, Committee Member

Lacy Ford, Senior Vice Provost and Dean of Graduate Studies

DEDICATION

This dissertation is dedicated to my parents, Jianwen Lu and Xiaochi Hu, whom give me unconditional love and make me who I am.

I also dedicate this work to my forever life partner, Brianna Cassidy, who is always there supporting me.

ACKNOWLEDGEMENTS

First of all, I would like to express the most sincere thanks to my Ph.D. advisor Dr. Stephen L. Morgan, who gave me tremendous help and support through my Ph.D. career. Working with him, taught me how to be a rigorous researcher and, most of all, how to be a better person.

I am lucky to have an admirable advisor, however, having an equally intelligent and supportive Co-PI at the same time is something you can only wish for. Dr. Michael Myrick was always the one who shone a light to my research when I encountered confusion and felt lost.

I would also like to acknowledge the other two of my committee members: Dr. Michael Angel and Dr. Blaine Griffen, for their advice and encouragement throughout my candidacy.

Last but not least, I would like to give thanks to families, friends, and colleagues, who were there and will always be there supporting me and helping me.

iv

ABSTRACT

Blood stains, which are among the traces encountered most frequently at crime scenes, are important for potential extraction and amplification of DNA for suspect identification, as well for spatter pattern analysis to reveal a sequence of events.

Attenuated total reflectance Fourier transform infrared spectroscopy (ATR-FTIR) was used in detection of blood stains and age estimation because of signature absorbances in the mid-infrared region at 3300 cm^{-1} (Amide A), 2800-3000 cm^{-1} (Amide B), ~1650 cm^{-1} (Amide I), ~1540 cm^{-1} (Amide II) ,and 1200-1350 cm^{-1} (Amide III).

Position and intensity shifts for amide peaks were observed due to aging changes occurring as a result of the denaturation of blood proteins and water absorption/desorption. Partial least square (PLS) regression was used in this work to combine these changes in a multivariate calibration for blood age estimation. Calibration experiments over several months at 30 ℃ under a variety of humidity and substrates enable prediction of blood stain age under different environmental conditions.

Amide peak intensity changes in the spectrum can be related to blood concentration. Multivariate calibrations of IR spectra of blood dilutions on four types of fabric (acrylic, nylon, polyester, and cotton) were built using PLS. Gap derivatives (GDs) were applied as a preprocessing technique to optimize the performance of calibration models. Detection limits of 0.028 μg/cm^2 for acrylic, 0.020 μg/cm^2 for nylon, 0.017 μg/cm^2 for polyester, and 0.0027 μg/cm^2 for cotton were found.

As a popular technique for rapid infrared spectra collection, ATR-FTIR requires samples to be compressed against an internal reflection element. However, depending on the accessory design, the pressure applied to the sample is not always well controlled. While collecting data from fabrics with heterogeneous coatings, we have observed systematic pressure-dependent changes in spectra that can be eliminated by reproducible pressure control. We describe a pressure sensor adapted to work with an ATR pressure tower to enable more rigorous control of pressure during ATR sampling.

TABLE OF CONTENTS

LIST OF TABLES

LIST OF FIGURES

CHAPTER ONE

USING FOURIER TRANSFORM INFRARED SPECTROSCOPY TO ESTIMATE BLOOD AGE UNDER DIFFERENT ENVIRONMENTAL CONDITIONS

ABSTRACT

Estimating the age of blood stains with good accuracy and precision has been an elusive goal for forensic investigations. Estimates of blood stain age can contribute to verify witness' statements, limit the number of suspects and confirm alibis. Fourier transform infrared spectroscopy (FTIR) can be used in forensic detection of blood stains and age estimation because of signature absorbance in the mid-infrared region at 3300 cm^{-1} (Amide A), 2800 cm^{-1} to 3000 cm^{-1} (Amide B), ~1650 cm^{-1} (Amide I), ~1540 cm^{-1} (Amide II) ,and 1200 cm^{-1} to 1350 cm^{-1} (Amide III). We have observed position and intensity shifts for these peaks due to age changes occurring as a result of the denaturation of blood proteins and water absorption/desorption. Partial least square regression (PLS) was used in this work to combine these changes in a multivariate calibration that reveals correlations between the amide peak changes and blood age. Calibration experiments over 83 days at 30 ℃ under a variety of humidity and substrate conditions enable prediction of blood stain age under different environmental conditions. This research contributes to the understanding of mechanisms of blood aging and provides a nondestructive and simple approach for predicting blood age under a variety of environmental conditions.

INTRODUCTION

Blood stains, which are among the traces encountered most frequently at crime scenes, are important for potential extraction and amplification of DNA for suspect

2

identification, as well for spatter pattern analysis to reveal a sequence of events.[1-6] Reconstruction of blood stain patterns at a crime scene can reveal a sequence of events.[4-6] The extraction and amplification of DNA can help identify possible suspects.[3,4] The estimation of the age of blood stains can also provide with probative forensic information regarding the time a crime was committed.[1,7]

In 1907, Tomellini developed a color chart to record the changing colors of blood over a period of a year.[7] Leers, in 1910, found that blood stains change from oxyhemoglobin (HbO_2) to methemoglobin (met-Hb), or a combination of the two products after drying and that their presence could be used to estimate blood age.[7] In the 1930s, Schwarzacher correlated the solubility of blood in water with its age. He also found that the intensity of catalase and peroxidase activity with hemoglobin was inversely related to the age of blood stains.[8] Hanson and Ballantyne found that a blue spectral shift of the hemoglobin Soret band at 414 nm in the UV/visible spectrum of blood is correlated with age of dried bloodstains.[9] In 2011, Bo Li, *et al.* reported the use of micro-spectrophotometry (MSP) to collect UV visible spectra of blood stains on white tile at wavelengths between 442 nm and 585 nm. After Fourier transformation of spectra, linear discriminant analysis was used to create a calibration model to predict blood aging.[10]

Inoue, *et al.* used high performance liquid chromatography (HPLC) to separate, identify and quantify the individual components in a blood stain, related the ratio of peak areas of hemoglobin α-chain and heme protein to blood aging. An unidentified peak at 220 nm, which not present in fresh blood, but related to blood age, was used to predict blood age out to 52 weeks.[11,12] HPLC was also used by Andrasko to estimate the age of

3

dried blood stains on cotton. The height of an unlabeled peak relative to a heme-related peak was employed for calibration, and the influence of humidity and temperature on prediction accuracy was discussed.[13]

Reflectance spectroscopy has also used in blood age estimation.[14,15] In the 1960s, Patterson recorded reflectance spectra of blood stains and determined that color changes of blood stains are related to environmental conditions.[14] The ratio of reflectance at 540 nm to that at 576 nm was employed by Kind, *et al.*[15] Near Infrared water peaks at 1359 nm and 1500 nm were reported to be able to estimate blood age within the first hour, while peaks at 1459 nm and 1900 nm due to the formation of met-Hb can be used for further predicting.[16]

Other techniques have been used to predict blood aging include oxygen electrodes to estimate the amount of HbO_2[17], electron paramagnetic resonance to measure a spin state change of iron ion in hemoglobin molecule[18], and atomic force microscopy(AFM) to measure Young's modulus of red blood cells.[19] However, despite these efforts, reliable estimation of blood age has been an elusive goal.

Blood Composition

Blood is composed of red blood cells, white blood cells, platelets and blood plasma. Protein comprises approximately 90% of red blood cells and 80% of plasma by weight. Oxygen-carrying protein hemoglobin makes up 97% of the blood's dry content.[20] In healthy blood, hemoglobin exists in two forms: deoxyhemoglobin (Hb), which is without oxygen, and oxyhemoglobin (HbO_2), which is saturated with oxygen. When blood is exposed to air, Hb is completely saturated with oxygen and converts to HbO_2.

4

HbO$_2$ will irreversibly oxidize to methemoglobin (met-Hb). After oxidization complete, met-Hb will denature to hemichrome (HC). These processes all cause changes in the secondary structure of the heme-related species.[7, 21]

Protein and its Secondary Structure

Protein is synthesized naturally from over 50 trans-amino acids. Amino acids are generally made up of carbon, oxygen, nitrogen, and hydrogen which are situated on a planar backbone (Figure 1.1). The sequence in which amino acids are linked is referred to as the primary structure of the protein.[18]

The secondary structure, or the conformation, of a protein refers to the 3-D folding of its peptide chain in space. A typical secondary structure of protein is the α-helix. About 80% proteins in hemoglobin are α-helix type. α-helix type of protein has 3.6 residues per turn. Due to the fact that every three to four amino acids apart in the backbone sequence are spatially closed, hydrogen bonds as well as van der Waals interactions will form between two closest amino acids as shown in Figure 1.2(A). Another regular conformation is β-sheet, which was displayed in Figure 1.2(B). Different form α-helix, β-sheet type protein has two residues per turn, and every two amino acids apart will form strong inter- and intra-molecular hydrogen bonds. Proteins that cannot fit in α-helix and β-sheet secondary structure will form random coil and loops.[22, 23]

Infrared Absorbance of Proteins

Mid-infrared spectroscopy is particularly well-suited for estimation of bloodstain age because fundamental absorption bands of blood protein are in this region.[20] As shown

5

in Figure 1.3, protein molecules have characteristic bands at 3300 cm^{-1}(amide A), 2800 cm^{-1}-3000 cm^{-1}(amide B), ~1650 cm^{-1}(amide I), ~1540 cm^{-1}(amide II) and 1200 cm^{-1}-1350 cm^{-1}(amide III).[24-27] Amide A and amide B vibrations originate from a Fermi resonance between the first overtone of amide II and the N-H stretching vibration.[24-27] These vibrational modes only depend on the backbone conformation, which are sensitive to the strength of hydrogen bonds or primary structure. The amide I peak is due to C=O stretching, which is directly related to the backbone conformation. The frequency of the C=O stretching band decreases as more hydrogen bonds are formed. The amide II peak is due to a combination of N-H bending (40%-60%), and C-N stretching (18%-40%). The amide III peak results from an in-phase combination of N-H in-plane bending and C-N stretching, and is usually a very weak resonance.[27]

The characteristic protein peaks, the amide I and amide II peaks, are sensitive to the secondary structures of a protein.[22,27,28] Amide I peaks in α-helix proteins are located at higher wavenumbers than either β-sheet proteins or random coil proteins (Table 1.1). As blood is exposed to air, the major proteins will unfold, and the secondary structure of proteins in blood will change from α-helix to β-sheet and form random coils. During this process, the IR absorbance at ~1650 cm^{-1} (amide I) and ~1540 cm^{-1} (amide II) will shift, accompanied by changes in intensities and peak shapes.[28]

6

METHOD

Sample Preparation

Three 4" × 11" acrylic and three 4" × 11" cotton samples were used as substrates. A 75% PVC/acetone mixture was used to create rings on fabric to limit the sampling area of blood. Mouse blood was received in a BD Vacutainer® vial (K2 EDTA, REF 367862, Franklin Lakes, NJ) from the Department of Animal Resources (University of South Carolina, Columbia, SC). The blood was deposited on fabric samples within 1 hr. of mouse expiration and blood extraction. Volumes of 200 μL of $100\times$ and $10\times$ diluted blood in distilled water, and of whole mouse blood were dispensed on the substrate fabrics using a micropipette within the containment rings (Figure 1.4). Three 6" × 12" glass tanks were used to create the artificial environment conditions for each sample. Saturated salt solutions in open beakers were used to create three levels of relative humidity of 65% ($NaNO_2$), 75% ($NaCl$), and 85% ($BaCl_2 \cdot 2H_2O$) at which aging experiments were conducted (Figure 1.5). Temperature and humidity were recorded using a Track-it® data logger (Amherst, NH).

IR Spectra Collection

Attenuated total reflectance Fourier transform infrared spectroscopy (ATR-FTIR) spectra were taken of all sets of samples every few days over 83 a day period. A Thermo Nicolet Nexus 670 Fourier transform infrared spectrometer (FT-IR) with a SmartDuraSamplIR (Thermo Scientific, Waltham, MA) attenuated total reflectance (ATR) accessory was employed. Three replicate spectra were collected for each ring

using 128 scans per collection at 4 cm^{-1} resolution over the wavenumber range of 400 cm^{-1} to 4000 cm^{-1}.

Data Processing

The Unscrambler X (CAMO software, AS) was used for data analysis. Savitzky-Golay smoothing was applied to all spectra by fitting a fourth polynomial with a window size 15 to reduce noise.[29] Smoothed spectra then were normalized by the standard normal variate transform (SNV). This requires each spectrum to be mean centered by subtracting the mean intensity of each spectrum from all elements. Each element of each spectrum is then divided by the standard deviation within the spectrum to normalize to unit length.[30] SNV preprocessing removes systematic variation due to different optical path-lengths between samples. Spectra from each set of environmental conditions and blood dilutions were mean centered before principal component analysis (PCA) and partial least squares regression (PLS) were applied to look at the discriminating ability for different blood dilutions, and to create prediction models for aging of bloodstains.

Partial least squares regression (PLS) finds a linear regression model by projecting predicted variables and observable variables to a new space, then find the fundamental relations between two matrices, construct a model explain the maximum covariance between two matrices.[31] Instead of using full spectra of proteins with different secondary structures, PLS uses "loading" vectors or "loading" spectra to reduce noises by distributing the noise through all "loading" vectors. The PLS model calibration is based on an X-block matrix containing the measured spectra, and a Y-block matrix containing corresponding information of X-block. X and Y-block were regressed using:

8

$$X = TP^T + E \qquad (1)$$

$$Y = UQ^T + F \qquad (2)$$

where X is an m×n data matrix of the spectra of the m calibration samples with n variables, P^T is an h×n matrix in which the rows comprise h PLS components with n variables each, called "loading" vectors generated by the PLS algorithm, T is a m×h matrix represent the intensities or scores of the h loading vectors in the new calibration system. E is an m×n matrix of spectral residuals not fit by the PLS model. Equation (2) shows that a similar analysis is performed for Y, producing a matrix of scores, U, loadings, Q, and residuals, F. The loading vectors in PLS models are composed of linear combinations of the original calibration spectra. The X matrix is reduced by only retaining those eigenvectors explaining a sufficiently large amount of covariance between X and Y.

PLS combines information from both X and Y matrices, an inner relationship, W, is built to relate scores of X to scores of Y

$$U = TW \qquad (3)$$

The fit of the model is optimized by exchanging the scores, T and U, in an iterative calculation, resulting in a PLS vector that maximizes covariance between the X and Y matrices. Once the model is calculated, a regression vector is calculated to predict the Y response (blood age):

$$B = P(P^TP)^{-1}WQ^T \qquad (4)$$

$$Y = XB \qquad (5)$$

We assessed the accuracy of PLS modelling using leave-three-out cross validation, in which three spectra is left out, in turn, and the remaining spectra in the data

9

matrix are used to re-construct the PLS regression model and to predict the spectra left out. The cross validated root mean square error of cross validation (RMSECV)

$$\text{RMSECV} = \left[\sum_k (y_k - \widehat{y_k})^2 / k \right]^{1/2} \qquad (6)$$

is a measure of prediction accuracy, where y_k and $\widehat{y_k}$ are the kth calibration data for actual and predicted age, respectively. The coefficient of determination, R^2, evaluates the proportion of total variation in Y explained by the calibration model,

$$R^2 = \frac{\sum_{k=1}^{n}(\widehat{y_k} - \bar{y})^2}{\sum_{k=1}^{n}(y_k - \bar{y})^2} \qquad (7)$$

where, $\widehat{y_k}$ are the predicted values of blood age, $\bar{y}$ is the mean of Y, y_k is the measured value of y.[31,32]

RESULTS AND DISCUSSION

For bloodstains on acrylic fabric subjected to 3 days of aging at different humidity levels, the projections of the principal component (PC) scores from the first two principal components are shown in Figure 1.6. The groups of replicate spectra taken from blood samples are separated in order of dilution level along the direction of the first PC. The first and second PCs account for 51% and 21% of the variance about the mean, respectively. Figure 1.7 shows a similar outcome for the corresponding PCA of spectra taken from blood samples on cotton fabric. However, variations of spectra due to age difference are not shown in PCA score plot, which indicates the necessity of calculating age related calibrations for spectra of varying dilutions separately.

Partial least squares regression was applied to spectra from different environmental conditions and dilutions on different substrates at different time periods to create calibration models for assessing the ability to predict age of a dried bloodstain. Figure 1.8 depicts a PLS prediction based on spectra taken from $10\times$ diluted bloodstains spectra on acrylic samples over a 20 day aging timeframe at 75% relative humidity. Each point on the figure represents a spectrum collected at the age corresponding to x axis value (day). Three replicate spectra were collected on each of the three replicate rings (9 spectra total) for each age. Three spectra from the same ring were left out for calculation of RMSECV. A good prediction with little variation was demonstrated in Figure 1.8. The coefficient of determination (R^2) for the fit of this model was 0.990, with a root-mean-square error of cross validation (RMSECV) of 0.654 day.

Table 1.2 summarizes R^2 and RMSECV values for PLS aging calibrations at different dilutions of blood stains on acrylic samples at different relative humidity conditions. Over a 20 day period, prediction uncertainties were limited within one to two days.

Figure 1.9 depicts the corresponding PLS calibration for age of $10\times$ diluted blood stains on cotton with 75% relative humidity for 21 days. R^2 of 0.961and RMSECV of 1.132 were achieved for this condition. Calibration statistics for PLS aging at different dilutions of blood stains on cotton samples at different relative humidity conditions are shown in Table 1.3. The R^2 values are slightly higher and RMSEC values lower than measured for bloodstains on acrylic.

PLS prediction for bloodstain age using IR spectra taken of bloodstains on acrylic up to 83 days are shown in Figure 1.10. At higher aging times, the replicate data increase

11

in variability, and the calibration statistics show a decrease in variation explaining (R^2), and increase in the RMSEC uncertainty estimates, which can lead to a possible assumption that blood aging process is a high order reaction, thus a nonlinear reaction behavior will challenge the prediction ability of PLS calibration (a linear calibration) as age increases.

Table 1.4 summarizes R^2 and RMSEC values for PLS aging calibrations up to 83 days at different dilutions of blood stains on (A) acrylic and (B) cotton samples at different relative humidity conditions. As bloodstains age longer, natural variability in the chemical changes that occur with time produces increased age calibration uncertainty. The coefficients of determination for the fitted models range from 0.825 to 0.964 for acrylic, 0.927 to 0.975 for cotton, with RMSEC values between 5 and 10 days for acrylic and 4 to 9 days for cotton.

Partial least squares regression prediction for age of blood on cotton achieved better results at both short and long time periods. Because cotton is a hydrophilic fabric, blood coating on cotton will be more homogeneous than on acrylic, which is hydrophobic. The resulting coating of blood will be more homogeneous on cotton samples, thus leading to a reduced variation of blood spectra collected on cotton samples. It is possible that the hydrophobic/hydrophilic nature of the substrate could also influence the mechanism if aging by promoting a different variety of interaction between blood and substrate.

12

CONCLUSIONS

ATR-FTIR was applied for estimation of bloodstain age over 83 days at different humidity levels on acrylic and cotton substrates. Partial least squares calibration was constructed to model systematic changes in peak intensity and position in the IR region associated with amide-related absorbance frequencies. Calibrations were calculated to predict blood stain age up to 20 days on acrylic samples with an error of 1-2 days, and an error of less than 2 day on cotton. For samples aged up to 83 days, age predictions produced uncertainties of 5-10 days for acrylic and 4-9 days for cotton.

An increased uncertainty was observed between short term prediction and long term prediction models, which suggests that blood aging process is possible a high order reaction. A nonlinear calibration is preferred in future work.

Differences in the chemical nature of the substrate surface, and they potential interactions of the substrate with blood, for acrylic compared to cotton may lead to variations of coating homogeneity that could alter the progress of blood aging. , which causes prediction of blood age on cotton demonstrated better performance than on acrylic.

ACKNOWLEDGEMENTS

13

www.manaraa.com

opinions, finding, and conclusions or recommendations expressed in the publication are those of the authors and do not necessarily reflect those of Department of Justice.

REFERENCES

(1) G. Edelman, V. Manti, S. M. Ruth, T. Leeuwen, M. Aalders. "Identification and Age Estimation of Blood Stains on Colored Backgrounds by Near Infrared Spectroscopy". *Forensic Sci. Int.* **2012.** 220: 239-244.

(2) J. N. McCutcheon. "Estimation of the Age of Bloodstains on Polymer Substrates by Infrared Spectroscopy". In preparation. **2015**.

(3) R. Bradshow, S. Bleay, M. R. Clench, S. Francese, "Direct Detection of Blood in Fingermarks by MALDI MS Profiling and Imaging". *Science and Justice.* **2014.** 54: 100-117.

(4) S.H. James, P.E. Kish, T.P. Sutton. "Principles of Bloodstain Pattern Analysis: Theory and Practice". 3rd ed. CRC Press. Boca Raton. **2005**.

(5) U.S. Department of Justice. "Forensic Sciences: Review of Status and Needs". AS Corporation. Gaithersburg, MD. **1999**.

(6) S. Richard. "A Simplified Guide To Bloodstain Pattern Analysis". In *Criminalistics: An Introduction to Forensic Science*. Pearson Education, Inc. Upper Saddle River, NJ. **2007.**

(7) R. H. Bremmer, K. G. Bruin, M. J. C. Gemert, T. G. Leeuwen. "Forensic Quest for Age Determination of Bloodstains". *Forensic Sci. Int*. **2012.** 216: 1-11.

(8) F. Schwarz. "Quantitative Analysis of Catalase und Peroxidase in Bloodstain". *Int. J. Legal Med.* **1937.** 27: 1-34.

(9) E. K. Hanson, J. Ballantyne. "A Blue Spectral Shift of the Hemoglobin Soret Band Correlates with the Age of Dried Bloodstains". *Plos ONE.* **2010.** DOI:10.1371/journal.pone.0012830.

(10) B. Li, P. Beveridge, W. T. O'Hare, M. Islam. "The Estimation of the Age of a Blood Stain Using Reflectance Spectroscopy with a Microspectrophotometer, Spectral Preprocessing and Linear Discriminant Analysis". *Forensic Sci. Int.* **2011.** 212: 198-204.

(11) H. Inoue, F. Takabe, M. Iwasa, Y. Maeno. "Identification of Fetal Hemoglobin and Simultaneous Estimation of Bloodstain Age by High-Performance Liquid Chromatography". *Int. J. Legal Med.* **1991.** 104: 127-131.

(12) H. Inoue, F. Takabe, M. Iwasa, Y. Maeno, Y. Seko. "A New Marker for Estimation of Bloodstain Age by High Performance Liquid Chromatography", *Forensic Sci. Int.* **1992.** 57: 17-27.

(13) J. Andrasko. "The Estimation of the Age of Bloodstains by HPLC Analysis". *J. Forensic. Sci.* **1997.** 42(4): 601-607.

(14) D. Patterson. "Use of Reflectance Measurements in Assessing the Color Changes of Aging Bloodstains". *Nature*. **1960.** 187: 688-689.

(15) S. S. Kind, D. Patterson, G. W. Owen. "Estimation of the Age of Dried Blood Stains by a Spectrophotometric Method". *Forensic. Sci.* **1972.** 1: 27-54.

(16) E. Botonjic- Sehic, C. W. Brown, M. Lamontagne, M. Tsaparikos. "Forensic Application of Near Infrared Spectroscopy: Aging of Bloodstains". *Spectrosc.* **2009.** 24: 42-48.

16

(17) T. Matsuoka, T. Taguchi, J. Okuda. "Estimation of Bloodstain Age by Rapid Determinations of Oxyhemoglobin by Use of Oxygen-electrode and Total Hemoglobin". *Biol. Pharm. Bull.* **1995.** 18: 1031-1035.

(18) T. Miki, A. Kai, M. Ikeya. "Electron Spin Resonance of Bloodstains and its Application to the Estimation of Time after Bleeding". *Forensic. Sci. Int.* **1987.** 35: 149-158.

(19) S. Strasser, A. Zink, G. Kada, P. Hinterdorfer, O. Peschel, W. M. Heckl. "Age Determination of Blood Spots in Forensic Medicine by Force Spectroscopy". *Forensic. Sci. Int.* **2007.** 170: 8-14.

(20) J. N. McCutcheon. "Forensic Discrimination, Age Estimation, and Spectral Optimization for Trace Detection of Blood on Textile Substrates Using Infrared Spectroscopy and Chemometrics". University of South Carolina. **2010.**

(21) W. J. Egan, W.E. Brewer, S. L. Morgan. "Measurement of Carboxyhemoglobin in Forensic Blood Samples Using UV/VIS Spectrometry and Improved Principal Component Regression," *Appl. Spectrosc.* **1999.** 53(2): 218-225.

(22) A. Mauerer. "Secondary Structural Change of Spray Dried Proteins with Fourier Transform Infrared Spectroscopy". Friedrich-Alexander University Erlangen-Nuremberg, Erlangen, Germany. **2006.**

(23) L. Pauling, R. B. Corey, H. R. Branson. "The Structure of Proteins; Two Hydrogen-Bonded Helical Configurations of the Polypeptide Chain." *Proc. Natl. Acad. Sci. U.S.A.* **1951.** 37(4): 205–11.

(24) K.M. Elkins. "Rapid Presumptive 'Fingerprinting' of Body Fluids and Materials by ATR FT-IR Spectroscopy". *J. Forensic. Sci.* **2011.** 56: 1580–1587.

17

(25) S. Cai, B. R. Singh. "Identification of β-turn and Random Coil Amide III Infrared Bands for Secondary Structure Estimation of Proteins". *Biophys. Chem.* **1999**. 80: 7-20.

(26) S. Cai, B. R. Singh. "A Distinct Utility of the Amide III Infrared Band for Secondary Structure Estimation of Aqueous Protein Solutions Using Partial Least Squares Methods". *Biochemistry*. **2004.** 43: 2541-2549.

(27) B. Smith. "Infrared Spectral Interpretation". CRC Press, Washington DC. **1999**.

(28) R. Krishnamoorthy, A. K. Mitra, M. D. In Taylor, G. L. Amidon, G. L. "Peptide-Based Drug Design-Contolling Transport and Metabolism". 47–68, Washington, DC. **1995.**

(29) A. Savitzky, M.J.E. Golay. ''Smoothing and Differentiation of Data by Simplified Least Squares Procedures''. *Anal. Chem.* **1964.** 36(8): 1627-1639.

(30) R.J. Barnes, M.S. Dhanoa, S.J. Lister. ''Standard Normal Variate Transformation and De-Trending of Near-Infrared Diffuse Reflectance Spectra''. *Appl. Spectrosc.* **1989.** 43(5): 772-777

(31) D. M. Haaland, E. V. Thomas. "Partial Least-Squares Methods for Spectral Analysis. 1. Relation to Other Quantitative Calibration Methods and Extraction of Qualitative Information". *Anal.Chem.* **1988.** 60: 1193-1202.

(32) S. D. Allison, T. W. Randolph, M. C. Manning, K. Middleton, A. Davis, J. F. Carpenter. "Effects of Drying Methods and Additives on Structure and Function of Actin: Mechanisms of Dehydration Induced Damage and its Inhibition". *Arch. Biochem. Biophys.* **1998.** 358(1): 171-81.

18

Table 1.1. Correlation between proteins structure and amide I frequency.[28]

Structural element	Amide I frequency [cm^{-1}]
α- helix	1648- 1660
β- sheet	1624- 1640
unordered	1640- 1648
Aggregated strands	1610- 1628

Table 1.2. PLS calibration statistics for age of bloodstains on acrylic, up to 20 days with different dilutions at different relative humidity.

R² / RMSECV	65%	75%	85%
100X	0.967	0.972	0.992
	1.196	1.102	0.586
10X	0.968	0.990	0.990
	1.184	0.654	0.649
Whole	0.971	0.974	0.982
	1.115	1.061	0.889

Table 1.3. PLS calibration statistics for age of bloodstains on cotton, up to 21 days with different dilutions at different relative humidity.

R^2 / RMSECV	65%	75%	85%
100X	0.975	0.977	0.983
	0.911	0.863	0.744
10X	0.970	0.961	0.989
	1.033	1.132	0.605
Whole	0.971	0.980	0.980
	0.986	0.814	0.803

Table 1.4. PLS calibration statistics for age of bloodstains on (A) acrylic and (B) cotton, up to 83 days with different dilutions at different relative humidity.

R^2 / RMSECV	65%	75%	85%
100X	0.937	0.947	0.917
	6.589	6.027	7.560
10X	0.964	0.957	0.955
	4.954	5.443	5.547
Whole	0.955	0.921	0.879
	5.545	7.339	9.096

(A)

R^2 / RMSECV	65%	75%	85%
100X	0.946	0.940	0.927
	6.437	6.963	7.534
10X	0.975	0.959	0.943
	3.784	5.592	6.947
Whole	0.941	0.932	0.909
	7.145	7.439	8.304

(B)

22
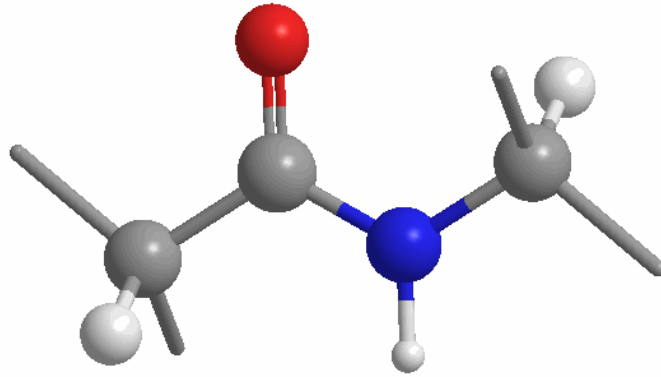
Figure 1.1. Geometry of the peptide backbone.
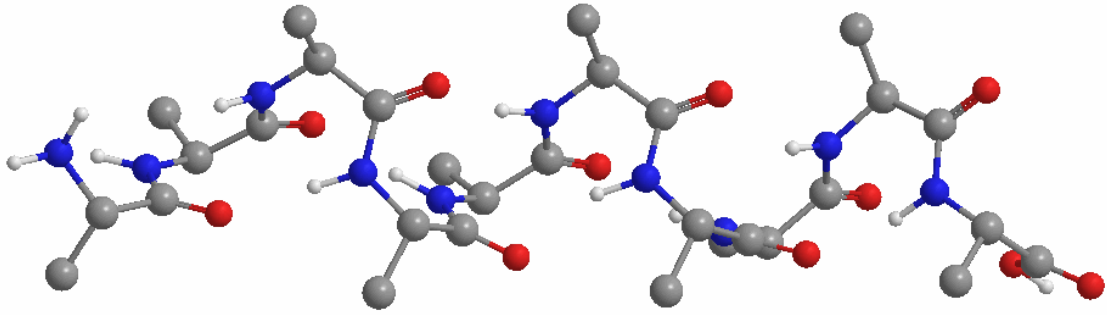
(A)
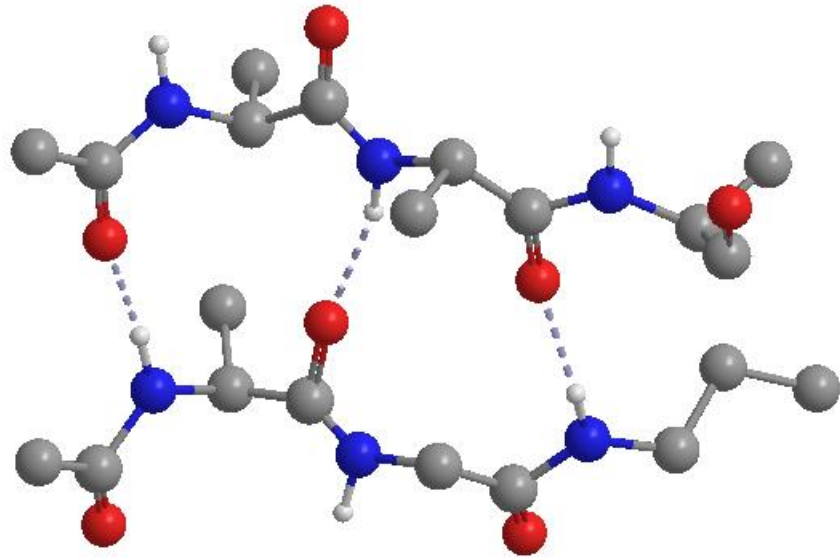
(B)

Figure 1.2. Secondary structure of protein: (A) α-helix. (B) β-sheet.
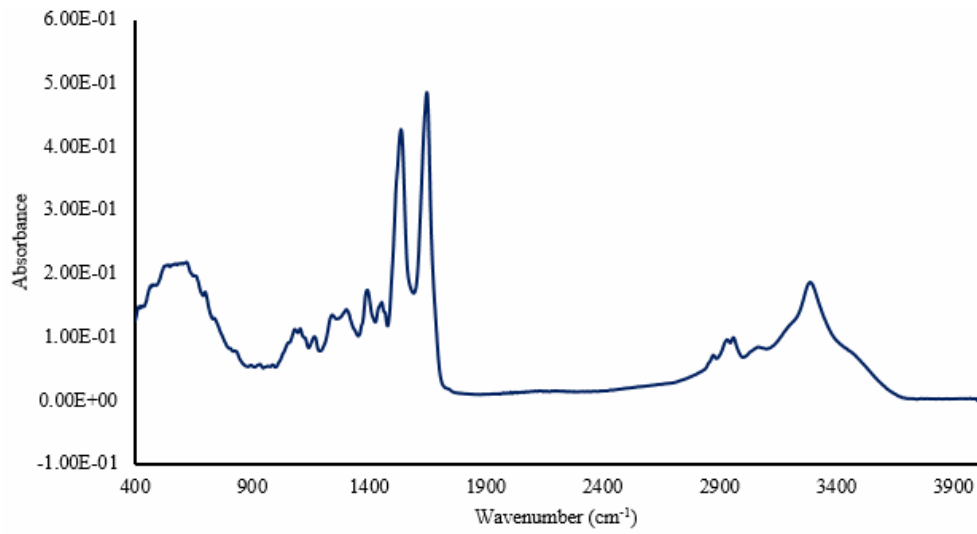
Figure 1.3. A spectrum of blood collected using attenuated total reflectance Fourier transform infrared spectroscopy.
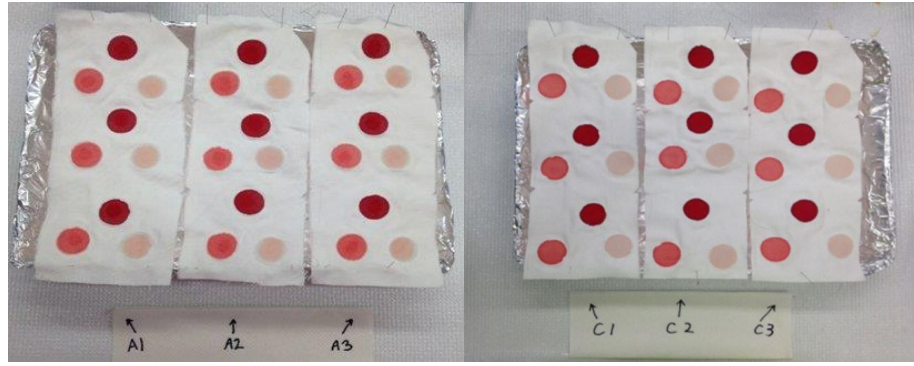
Figure 1.4. (Right) Three replicate acrylic samples, and (left) three replicate cotton samples doped with blood at varying dilution factors.

Figure 1.5. Artificial aging environment created with glass tanks (side and top views).
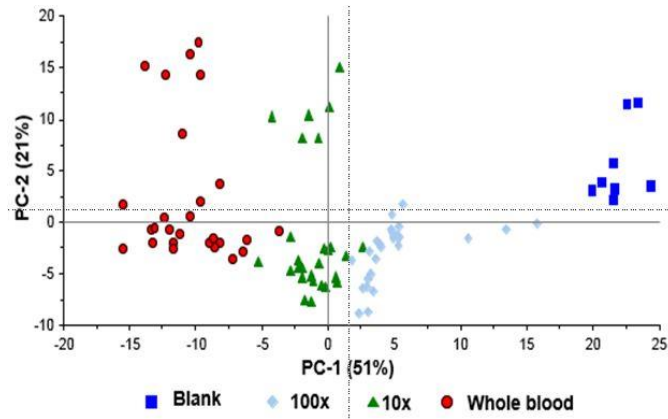
Figure 1.6. Principal component projections of spectra taken from acrylic samples coated with blood and held at 65% relative humidity after the third day of artificial aging.
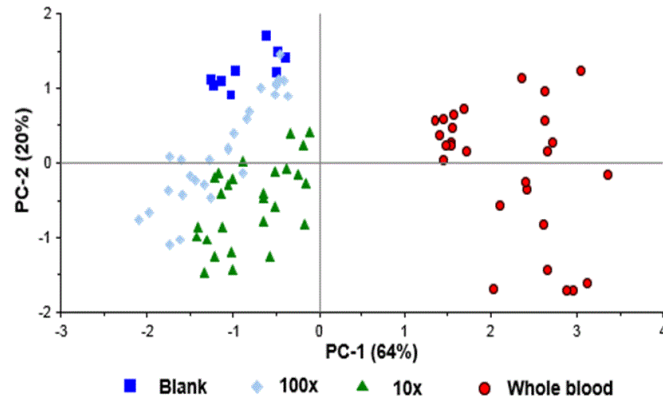
Figure 1.7. Principal component projections of spectra taken from cotton samples coated with blood and held at 65% relative humidity after the third day of artificial aging.
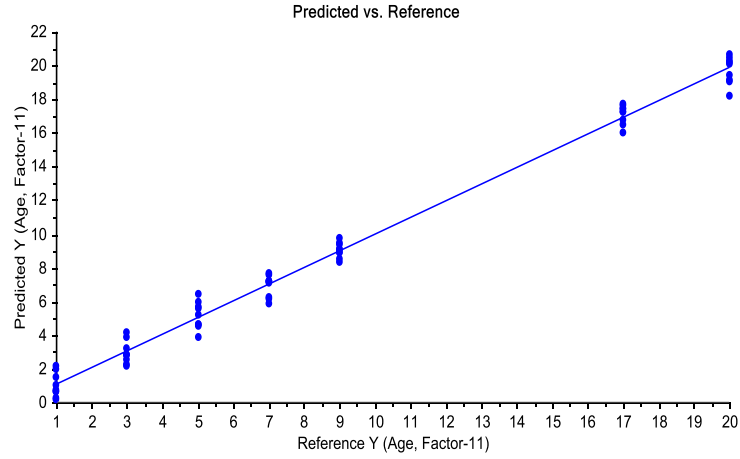
Figure 1.8. PLS calibration for age of bloodstains, based on ATR-FTIR spectra from 10× diluted bloodstains on acrylic at 75% relative humidity for 20 days.

30
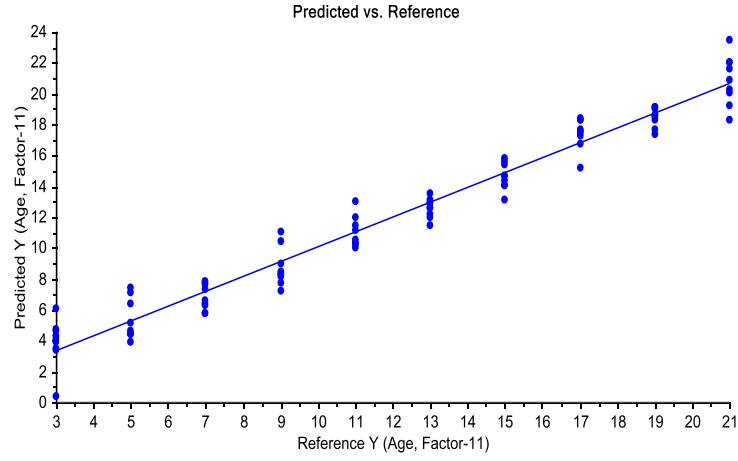
Figure 1.9. PLS prediction based on ATR-FTIR spectra from $10 \times$ diluted bloodstains on cotton at 75% relative humidity for 21 days.
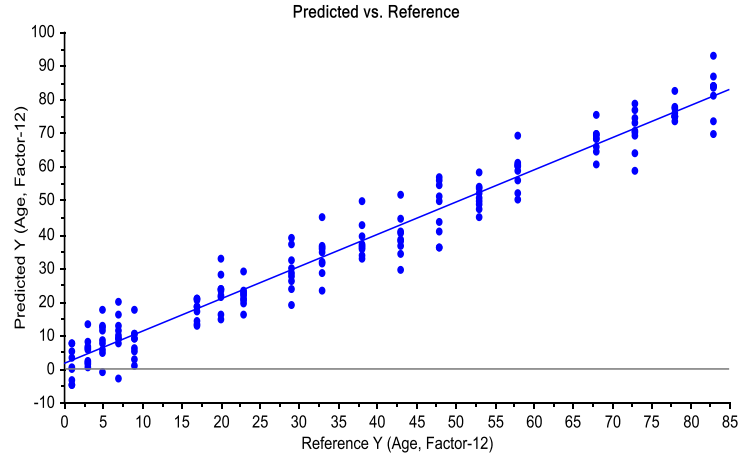
Figure 1.10. PLS calibration based on ATR-FTIR spectra from 10× diluted bloodstains on acrylic at 75% relative humidity for 83 days. The coefficient of variation was 0.957 and RMSEC was 5.443 days.

.

CHAPTER TWO

DETECTION LIMITS FOR BLOOD ON FABRICS USING
ATTENUATED TOTAL REFLEC-TANCE INFRARED
SPECTROSCOPY AND DERIVATIVE PROCESSING

ABSTRACT

Blood stains, one of the most common types of trace evidence found at crime scenes, are important for DNA analysis, which might identify suspects, and for blood spatter analysis, which might reveal event sequence. Attenuated total reflectance Fourier transform infrared spectroscopy (ATR-FTIR) was used to detect blood stains based on signature protein absorption in the mid-infrared region, where intensity changes in the spectrum can be related to blood concentration. Partial least squares regression (PLSR) was applied for multivariate calibrations of IR spectra of blood dilutions on four types of fabric (acrylic, nylon, polyester, and cotton). Gap derivatives (GDs) were applied as a preprocessing technique to optimize the performance of calibration models. Detection limits of 0.028 μg/cm^2 for acrylic, 0.020 μg/cm^2 for nylon, 0.017 μg/cm^2 for polyester, and 0.0027 μg/cm^2 for cotton were found.

INTRODUCTION

Blood stain detection at crime scenes has great forensic value.[1-4] Identification of blood stains allows verification of witness statements, identification of potential suspectsand information about the nature of the crime.[5] This information is obtained by DNA analysis of blood stains and by blood spatter analysis.[3,4,5]

Attenuated total reflectance Fourier transform infrared spectroscopy (ATR-FTIR) has been used to identify and study blood stains by examining signature protein absorbances in the mid-infrared region at 3300 cm^{-1} (Amide A), 2800 cm^{-1} to 3000 cm^{-1} (Amide B), ~1650 cm^{-1} (Amide I), ~1540 cm^{-1} (Amide II), and 1200 cm^{-1} to 1350 cm^{-1}

34

(Amide III)[6,7,8] Intensities of these amide peaks vary with blood concentration, enabling calibration for blood concentration and estimation of a detection limit (DL) for blood using ATR-FTIR spectroscopy.

Previous work done by DeJong, *et al.* used gap derivative (GD) processing combined with partial least squares regression (PLSR) to build multivariate calibrations for diffuse reflectance infrared spectra of blood collected on different fabric types (acrylic, nylon, polyester, and cotton).[9,10] While diffuse reflectance spectroscopy produced good DLs ($\sim 1000 \times$ dilute blood on acrylic, polyester, and cotton fabrics), ATR-FTIR might be better suited for detection of blood on surfaces of samples due to its inherent surface sensitivity.[6] ATR shares the advantages of diffuse reflection, including the small sampling area, little-to-no sample preparation, and being non-destructive. Further, ATR-FTIR offers a small penetration depth less than 10 microns compared to greater than 1.5 mm for diffuse reflection.[11] A shortened penetration depth enables detection of even small amounts of blood on surfaces of highly absorbing substrates, such as fabric.

The present research replicates the statistical methods of our previous work performed on ATR-FTIR spectra collected from the same samples.[10] To facilitate comparisons between the two techniques, we report the DL in units of mass per area ($\mu g/cm^2$), as well as the more commonly employed units of dilution factor.

METHOD

Fabric Samples

Five replicate samples with a size of 2″ × 2″ were prepared for each of the four fabric samples (acrylic, cotton, nylon and polyester) at one blood dilution level. Five dilution levels (25×, 50×, 100×, 200×, and blank) were applied. All fabric samples were sonicated for 60 min in deionized water and suspended to dry for 24 h before dip coating in diluted rat blood. All samples were allowed hang at room conditions until dry before spectral collection.[9,10]

IR Spectra Collection

A Thermo Nicolet IS5 Fourier transform infrared spectrometer (FT-IR) with an ID3 ATR accessory (Thermo Scientific, Waltham, MA) was employed. A 7 mm diameter germanium crystal with a 45 ° incident angle was used as the totally reflective element. Twenty replicate spectra were collected of each fabric using 64 scans at 4 cm^{-1} resolution over the wavenumber range of 600 cm^{-1} to 4000 cm^{-1}. Spectra were collected over five consecutive days, with one sample square of each dilution measured each day.

Data Processing

Gap derivative processing was performed using in-house code developed in Matlab® (The MathWorks, Inc., Natick, MA). Calibrations were developed using PLSR using the PLS Toolbox 6.7.1 (Eigenvector Research, Wenatchee, WA).

36

First gap derivative (First GD), second gap derivative (Second GD) and fourth gap derivative (Fourth GD) processing were applied on all spectra. Gap sizes between 1-50 points (1.93-96.4 cm^{-1}) were selected for this work as previously done. Derivative spectra were trimmed to three different wavelength regions: full spectra (600 cm^{-1} to 4000 cm^{-1}), Amide I-II region (1400 cm^{-1} to 1900 cm^{-1}), and Amide A-B region (2688 cm^{-1} to 3614 cm^{-1}) for calibration modeling.

The standard normal variate transform (SNV) was applied to all spectra. Eighty spectra of each fabric type of each dilution (taken over a 4-day period) were selected as a calibration set (400 calibration spectra). The remaining 20 spectra (taken over 1 day) were selected as a validation set (100 validation spectra). Because of non-linear effects in the calibration models at higher concentrations, detection limits were calculated from the slope of the validation set across the blank, 200×dilute, and 100×dilute samples of the validation set.[10] Detection limits were estimated by Equation 1.

$$\text{DL} = \frac{1}{3 \times \sigma_{\hat{y}} \Big/ m_{y,\hat{y}}} \qquad (1)$$

where $\sigma_{\hat{y}}$ is the standard deviation of the predicted values of the blank samples, and $m_{y,\hat{y}}$ is the slope of the linear fit between the model reference and predicted values.[12,13] The $3\sigma_{\hat{y}}$ detection limit multiplier corresponds to a 0.14% false positive rate assuming normally distributed measurement errors.

Fabric Thickness

To convert the DLs for ATR calibrations from units of dilution factor to coverage of blood solids, it is necessary to know the effective thicknesses of different fabrics.

37

Fabric effective thickness was evaluated by pressing the fabric between two glass slides by the ATR pressure tower as shown in Figure 2.1. Total thickness of the two glass slides, pressure sensor, and fabric was measured using calipers. The effective fabric thickness was obtained by subtracting the thickness of glass slides and pressure sensor under the same pressure. The pressure sensor ensured that the pressure applied to the fabric was consistent across spectral collection.

Model Selection

One inconvenient point of using GDs as a preprocessing method is that, due to the possibility of using different gap size combinations, a large number of models are generated, which have to be evaluated. For example, 1-50 points were selected as possible gap sizes in this work, which resulted in 25 models for First GD, 350 models for Second GD, and 13925 models for Fourth GD.[9]

Due to the large number of potential models, a screening method is necessary to evaluate the models for optimal performance based on user-defined calibration metrics. The RPD, or the ratio of the standard deviation of the reference value to the root mean square error of prediction (RMSEP), is a convenient metric to evaluate model predictive ability. The RPD was first introduced by Williams, et al., who suggested RPD greater than 3 is an acceptable screening limit to judge model quality.[14] However, RPDs greater than 2 have also been used as an acceptable performance criterion.[15,16] For this work, RPD values were used to describe models as excellent (RPD $\geq$ 3), fair (3 > RPD $\geq$ 2.5), or poor (RPD < 2.5).

38

For models exhibiting excellent performance, the reported DL for each fabric is that having the lowest detection limit (*i.e.*, higest dilution). If no models show an RPD ≥ 3, the reported DL for each fabric is that having the lowest detection limit (*i.e.*, higest dilution) within the fair performance range. If all models for a fabric demonstrate poor performance, DLs are not reported.

Detection Limit Unit Conversion

As mentioned previously, an advantage of ATR-FTIR in blood detection over diffuse reflection spectroscopy is that ATR-FTIR is more surface sensitive. DLs reported in units of dilution factor or mass percentage will not fairly compare the two techniques, particularly in cases where blood is concentrated on the surface of fabric rather than spread throughout the bulk fabric. We have chosen to use units of coverage ($\mu g/cm^2$) to compare the two techniques so as to better account for the fact that ATR measures absorbance at lower penetration depth. The penetration depth (d_p) of the ATR sampling area is calculated as

$$d_p = \frac{\lambda}{2\pi(\eta_1^2 \sin^2\theta - \eta_2^2)^{1/2}} \qquad (2)$$

where λ is wavelength of light (an averaged wavelength over the selected wavelength region), θ is the angle of incidence (45°), η_1 is the refractive index of the ATR crystal (4.00, for germanium), and η_2 is the refractive index of the sample.[11] Table 2.1 list refractive indices and calculated penetration depths in several IR regions for fabrics used in this work.[17]

Our previous work suggests that, regardless of fabric thickness, there is a linear relationship between blood solid coverage (mg/cm^2) and the 1/dilution factor (Table 2.2). The average thickness of each fabric is summarized in Table 2.3.

When the effective film thickness is taken into account, Equation 3 can be used to estimate coverage units from the dilution factor:

$$BSC = \frac{S \times d_p}{DF \times Tf} \times 1000 \qquad (3)$$

where *S* is the slope of the linear relationship shown in Table 2.2, *DF* is the *DL* in unit of dilution factors, and *Tf* is fabric thickness.

DISCUSSION

Calibration Results

Figures 2.2-2.5 summarize best models for the four fabrics in units of dilution factor (left axis) and blood solid coverage (right axis, μg/cm^2). In each figure, the bar graph values are shown on the left axis, are separated into three groups, corresponding to the models selected on first, second, and fourth gap derivatives. Light grey, medium grey, and dark grey bars represent the respective models based on the full IR spectra region (600 cm^{-1} to 4000 cm^{-1}), Amide I-II region (1400 cm^{-1} to 1900 cm^{-1}), and Amide A-B region (2688 cm^{-1} to 3614 cm^{-1}). Numbers above each bar provide the RPD and gap sizes employed for each model, and the bar representing the model having the lowest DL is outlined in black. Data connected by the black line corresponding dilution factor converted to the units of blood solid coverage (shown on the right axis). The detection limits, in dilution factor units, for blood on the four fabrics were 268 for acrylic, 249 for

40

nylon, 282 for polyester, and 2707 for cotton. Converted to blood solid coverage units, these values correspond to 0.028 µg/cm^2 for acrylic, 0.020 µg/cm^2 for nylon, 0.017 µg/cm^2 for polyester, and 0.0027 µg/cm^2 for cotton. These results are further discussed separately for each fabric in the following sections.

Acrylic. Calibration models for blood concentration on acrylic in all cases were "excellent" or "fair" models. According to the model selection rules stated above, the best model for acrylic was found in the amide I-II region using fourth GD processing with a detection limit of 0.028 µg/cm^2 (268×). This spectral region is where amide peaks show strong absorbance, while interference from acrylic bands is small.

Models for blood on acrylic using fourth GDs are better than those using first GDs and second GDs, probably because ATR-FTIR spectra of blood-coated acrylic fabrics exhibit narrow features accompanied by high frequency noise. Thus, narrow gap sizes that would normally highlight relevant spectral features also increase noise. Conversely, broad gaps that usually smooth the high-frequency noise also suppress the analyte signal. As a result, it is difficult to find a single gap size (first GD), or a simple combination of gaps (second GD), to improve the calibration.

Figure 2.6 shows a plot of predicted vs. actual dilution factors for the selected PLSR model based on three latent variables over the amide I-II region using fourth gap derivatives with gap sizes of 10, 12, 32, 34. At blood concentration on the fabric increases, the variability of the predictions also increase.

One explanation for this phenomenon could be that dip-coating fabrics from more concentrated blood solutions results in a more heterogeneous coating because of the hydrophobicity of acrylic fabric.[17] ATR-FTIR is very sensitive to coating effects on

41

substrates, and the increased variability of spectra at higher blood concentrations may be due to fabric/coating variability. Because RPD values are influenced by the general prediction error, RPD will suffer from poor predictions of the most concentrated samples, even if prediction of the more dilute samples is accurate. One way to account for this phenomenon might be to estimate DLs as multivariate limits of detection rather than by pseudounivariate estimates.[18] Multivariate DL estimators might be able to compensate for variability in actual values of dilution which might be caused by fabric/coating inhomogeneity.

Nylon. In previous work, valid calibrations could not be found for blood on nylon fabric.[10] Because of the large sampling depth of diffuse reflectance, the similarity of IR spectra of blood and nylon is hard to overcome even with the increased sensitivity offered by fourth GD processing. As shown in Figure 2.3, the present calibration models (calculated based on ATR-FTIR spectra of the previous set of nylon samples) suffer from the same problem. However, due to the increased surface sensitivity offered by the small penetration depth of ATR-FTIR, this technique has the potential to identify less intense amide peaks on the fabric surface. Our current results produce fair models for blood on nylon in the Amide I-II region, with a DL of 0.020 μg/cm^2 (249×). As shown in Figure 2.7, the selected model is able to predict test spectra accurately at all levels of blood dilution. This case demonstrates the advantage of using ATR-FTIR in the situation where the substrate spectrum heavily interferes with the spectrum on the analyte coated on the surface.

Polyester. Models of blood on polyester with excellent detection limits were found in the previous work, with the best results occurring in the amide A-B region.[10]

Our present best DL for blood on polyester of 0.017 μg/cm^2 (282×) is also found in the amide A-B region (Figure 2.4). However, as before, the model RPD are only 'fair' for polyester. The behavior of the predicted values of these calibrations is different than that of acrylic, though difficulties in developing good calibrations is likely rooted in similar sources of sample variability. While acrylic predictions were worse at higher concentrations, the predictions for blood on polyester are worse at low blood concentrations (Figure 2.8). Polyester is more hydrophobic than acrylic fabric[17], so dip-coating is less effective in creating a uniform coating; a greater amount of blood must be present in the solution before the blood will evenly adsorb to the fabric. Thus, even though spectra of polyester do not interfere with that of blood, the calibrations are once again only 'fair.' In this case, the advantages of ATR-FTIR become disadvantages: techniques with larger sampling area and depth are needed to detect blood on the non-uniformly coated polyester samples.

   Cotton. Blood on cotton produced models with the best limits of detection (0.0026 μg/cm^2, 2707×) in this work. Cotton does not suffer the same problems in sample preparation as polyester and acrylic stated above (Figure 2.9). This enables the development of excellent calibration models and correspondingly excellent estimates for the DL. Models built on the amide I-II region are better in comparison to those built on the amide A-B region. Averaged spectra show that amide A-B peaks are obscured by hydroxyl peaks from cotton fabrics, while cotton shows minimal interference with the amide I-II bands.

CONCLUSIONS

This work, based on detection of blood on fabrics using ATR-FTIR, offers a contrast to our previously reported results on detection of blood using diffuse reflectance measurements. The smaller penetration depth and sample area associated with ATR-FTIR has demonstrated the difficulty of creating a uniform coating on hydrophobic fabrics, which complicates the development of high-quality PLSR models. These complications might be mitigated using multivariate-based limit of detection estimators, rather than the pseudounivariate approach used here. Detection limits were found at dilution factor of 268 for acrylic, 249 for nylon, 282 for polyester, and 2707 for cotton in this work. When converted to blood solid coverage unit, limits of detection was found to be 0.028 $\mu g/cm^2$ for acrylic, 0.020 $\mu g/cm^2$ for nylon, 0.017 $\mu g/cm^2$ for polyester, and 0.0027 $\mu g/cm^2$ for cotton. These numbers are several magnitudes smaller than previously reported in the literature.

ACKNOWLEDGEMENTS

REFERENCES

(1) J. N. McCutcheon. "Forensic Discrimination, Age Estimation, and Spectral Optimization for Trace Detection of Blood on Textile Substrates Using Infrared Spectroscopy and Chemometrics". University of South Carolina. **2010**.

(2) R. Bradshow, S. Bleay, M. R. Clench, S. Francese. "Direct detection of blood in fingermarks by MALDI MS profiling and Imaging". *Science and Justice*. **2014.** 54: 100-117.

(3) S.H. James, P.E. Kish, T.P. Sutton. "Principles of Bloodstain Pattern Analysis: Theory and Practice". 3rd ed. CRC Press, Boca Raton. **2005**.

(4) U.S. Department of Justice. "Forensic sciences: review of status and needs". Gaithersburg, MD. AS Corporation. **1999**.

(5) R. Saferstein. "Criminalistics: An Introduction to Forensic Science". Pearson Education, Inc., Upper Saddle River, NJ. **2007**

(6) K.M. Elkins, "Rapid Presumptive 'Fingerprinting' of Body Fluids and Materials by ATR FT-IR Spectroscopy". *J. Forensic Sci.* **2011.** 56: 1580–1587.

(7) S. Cai, B. R. Singh. "Identification of β-turn and Random Coil Amide III Infrared Bands for Secondary Structure Estimation of Proteins". *Biophys. Chem.* **1999**. 80: 7-20.

(8) S. Cai, B. R. Singh. "A Distinct Utility of the Amide III Infrared Band for Secondary Structure Estimation of Aqueous Protein Solutions Using Partial Least Squares Methods". *Biochemistry*. **2004.** 43: 2541-2549.

45

(9) S. A. DeJong, W. L. O'Brien, Z. Lu, B. M. Cassidy, S. L. Morgan, and M. L. Myrick. "Optimization of Gap Derivatives for Measuring Blood Concentration of Fabric from Vibrational Spectroscopy". *Appl. Spectrosc.* **2015**. 69(6): 733-748.

(10) S. A. DeJong, Z. Lu, B. M. Cassidy, W. L. O'Brien, S. L. Morgan, M. L. Myrick. "Detection Limits for Blood on Four Fabric Types Using Infrared Diffuse Reflection Spectroscopy in Mid- and Near-Infrared Spectral Windows". *Anal. Chem.* **2015**. DOI: 10.1021/acs.analchem.5b01825.

(11) N. J. Harrick. "Internal Reflection Spectroscopy". Interscience Publishers, New York. **1967**.

(12) L. Currie. Nomenclature in Evaluation of Analytical Methods Including Detection and Quantification Capabilities". *Pure Appl. Chem.* **1995.** 67: 1699-1723.

(13) R. Boque, F. X. Rius. "Multivariate Detection Limits Estimators". *Chemom. Intell. Lab. Syst.* **1996.** 32: 11-23.

(14) P.C. Williams. ''Implementation of Near-Infrared Technology''. In: P.C. Williams, K.H. Norris, editors. Near-Infrared Technology in the Agricultural and Food Industries. St. Paul, MN: American Association of Cereal Chemists, **2001**. Ch. 8, Pp. 145-170.

(15) C. W. Chang, D. A. Laird, M. J. Mausbach, C. R. Hurburgh. "Near Infrared Reflectance Spectroscopy - Principal Components Regression Analyses of Soil Properties". *Soil Science society of America journal*. **2001.** 65: 480-490.

(16) V. Bellon-Maurel, E. Fernadez-ahumada, P. Palagos, J. M. Roger, A. B. McBratney. "Critical Review of Chemometric Indicators Commonly Used for

46

Assessing the Quality of the Prediction of Soil Attributes by NIR Spectroscopy".

*Trends Anal. Chem.***2010.** 29: 1073-1081.

(17)W. E. Morton, J. W. S. Hearle, "Physical Properties of Textile Fibres". Fourth edition. CRC Press. Washington, DC. **2008.**

(18)F. Allegrini, Al. C. Olivieri. "IUPAC- Consistent Approach to the limit of detection in Partial Least Squares Calibration". *Anal. Chem.* **2014.** 86: 7858-7866.

Table 2.1. Penetration depth for fabrics.

Fabric	η_1	d_p, full spectrum (μm)	d_p for amide I-II (μm)	d_p for amide A-B (μm)
Acrylic	1.500	0.289	0.402	0.211
Nylon	1.551	0.293	0.408	0.214
Polyester	1.631	0.300	0.417	0.219
Cotton	1.555	0.293	0.408	0.214

48

Table 2.2. Conversion factors of 1/dilution factor to blood solid coverage (mg/cm^2) for different fabric types

Fabric	Conversion Factor of 1/Dilution Factor to Blood Solid Coverage (mg/cm^2)
Acrylic	43.5
Nylon	33
Polyester	26
Cotton	30

Table 2.3. Average thickness of different fabric types.

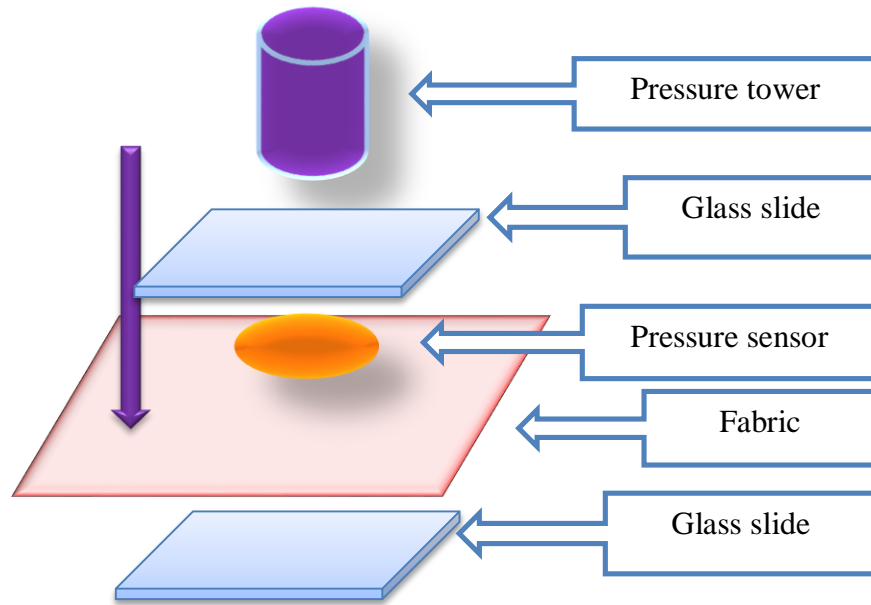| Fabric	Effective fabric thickness (mm)
Acryic	0.716
Nylon	0.738
Polyester	0.171
Cotton	0.468

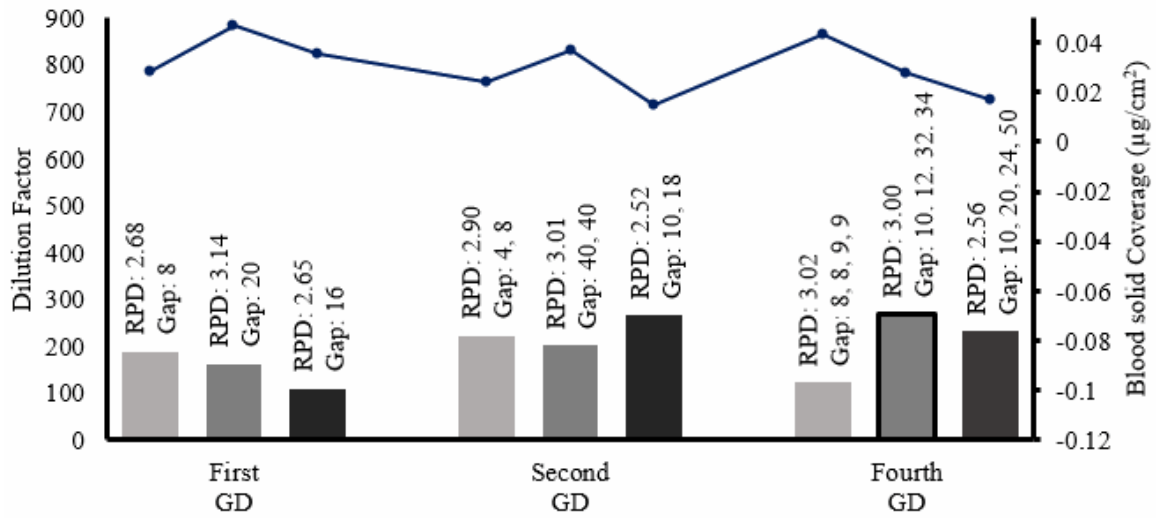**Figure 2.1.** Schematic for measuring fabric thickness.

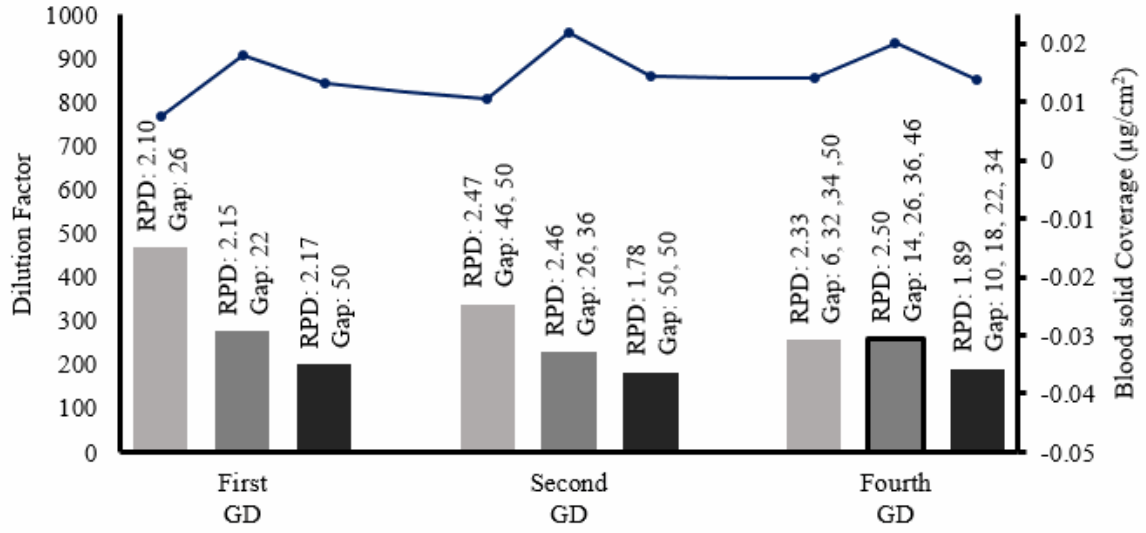**Figure 2.2.** Summary of the best PLSR models for acrylic.
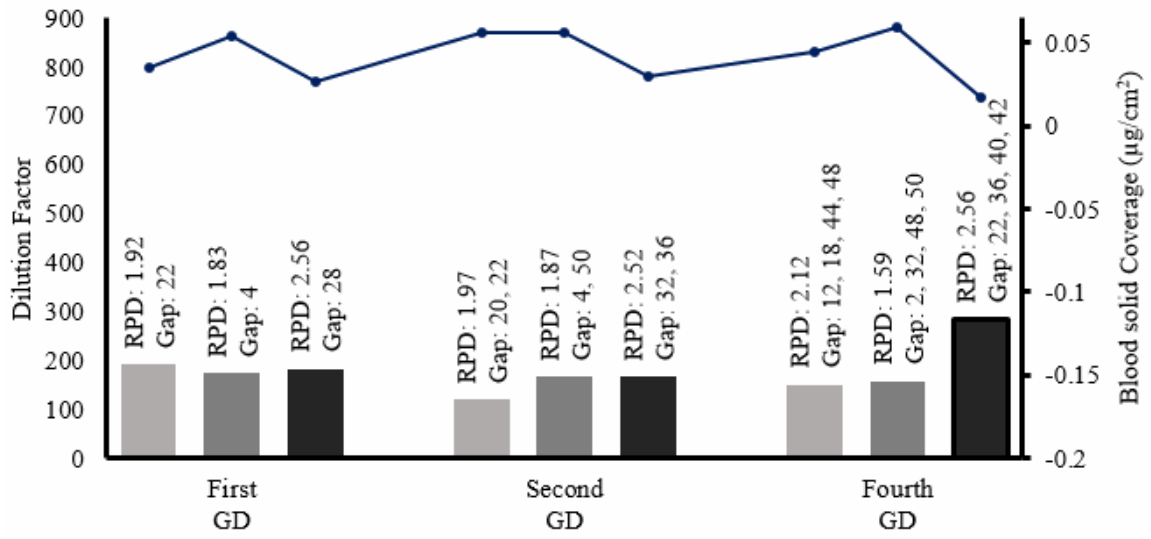
Figure 2.3. Summary of the best PLSR models for nylon.

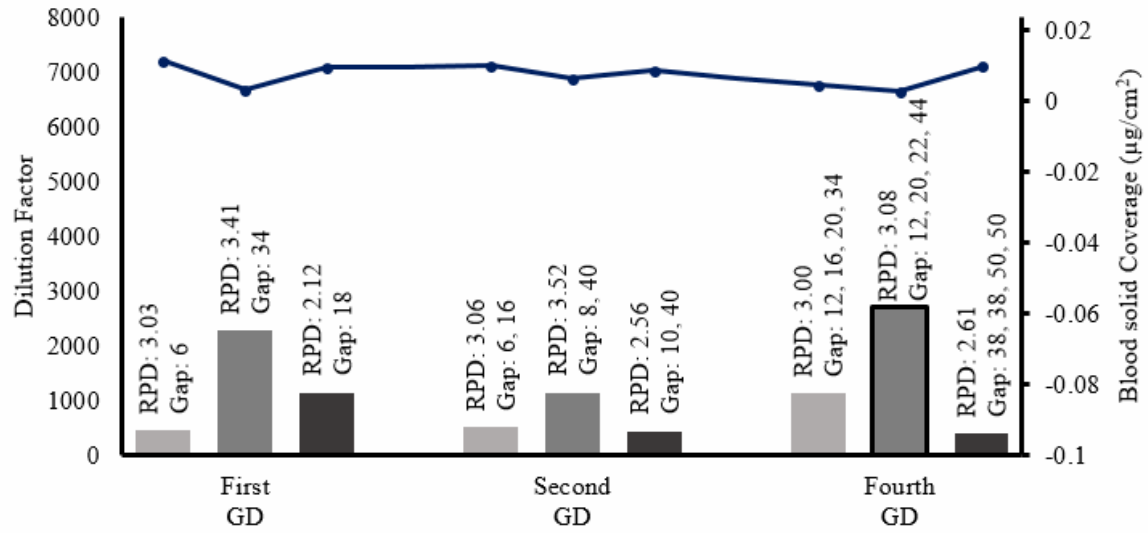**Figure 2.4.** Summary of the best PLSR models for polyester.

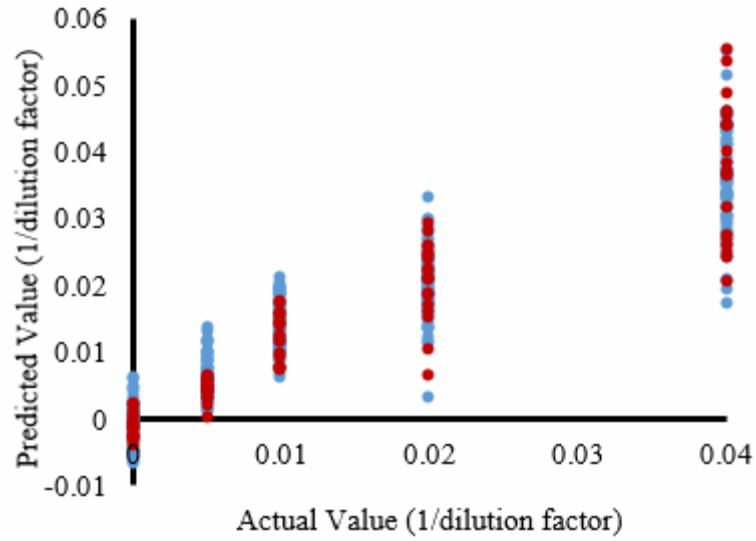**Figure 2.5.** Summary of the best PLSR models for cotton.

Figure 2.6. PLSR prediction of dilution factor for blood on acrylic based on the amide I-II region using fourth gap derivatives (gap sizes: 10, 12, 32, 34). Light dots represent calibration set (400 spectra), and dark dots represent test set (100 spectra) data.
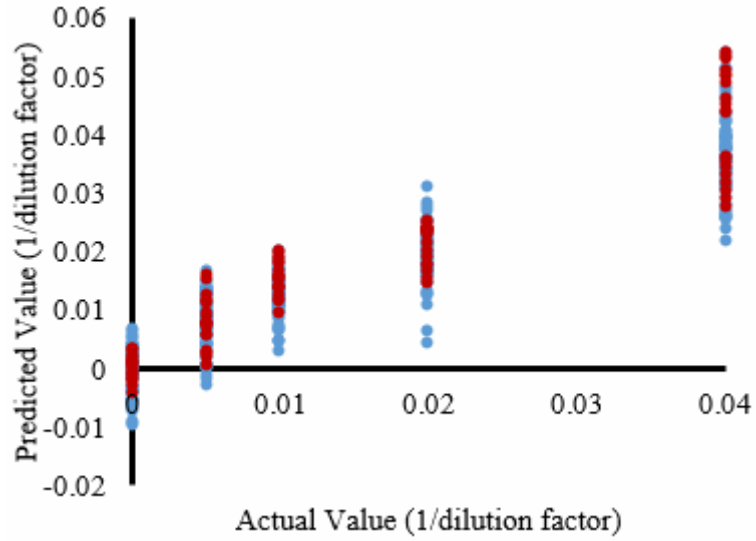
56

Figure 2.7. PLSR prediction of dilution factor for blood on nylon based on the amide I-II region using fourth gap derivatives (gap size:14, 26, 36, 46). Light dots represent calibration set (400 spectra), and dark dots represent test set (100 spectra) data.
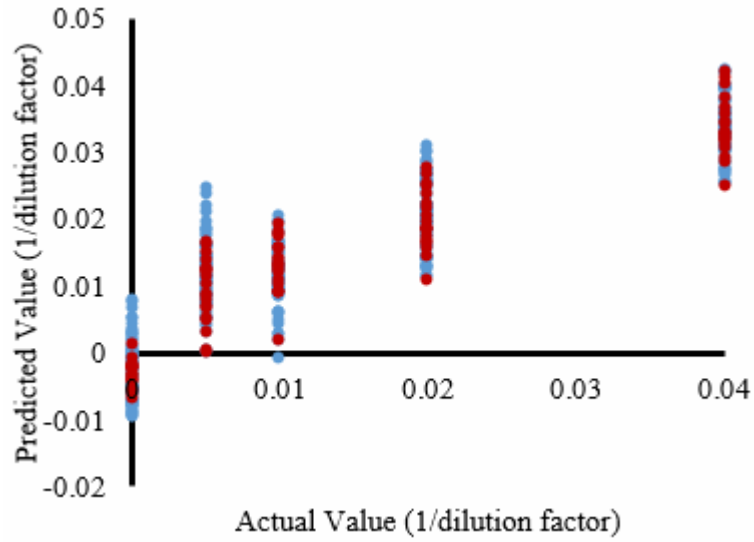
Figure 2.8. PLSR prediction of dilution factor for blood on polyester based on the amide A-B region using fourth gap derivatives (gap size: 22, 36, 40, 42). Light dots represent calibration set (400 spectra), and dark dots represent test set (100 spectra) data.

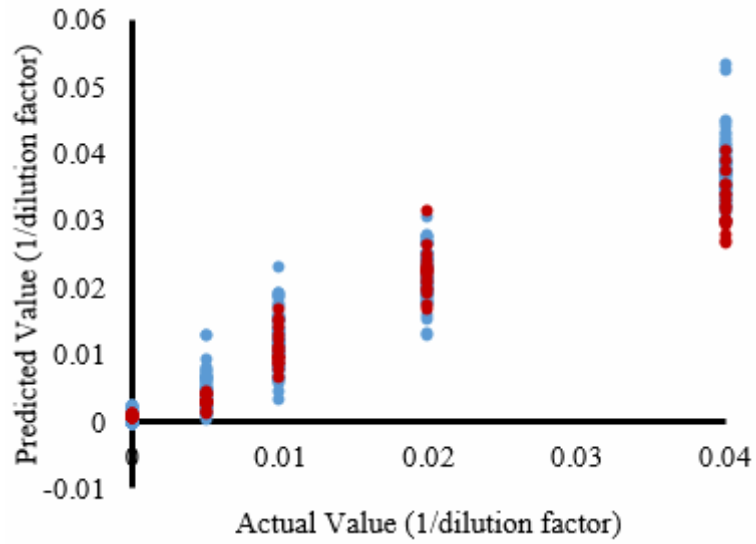**Figure 2.9.** PLSR prediction of dilution factor for blood on cotton based on the amide I-II region using fourth gap derivatives (gap size:12, 20, 22, 44). Light dots represent calibration set (400 spectra), and dark dots represent test set (100 spectra) data.

CHAPTER THREE

ATTENUATED TOTAL REFLECTANCE SAMPLING IN

INFRARED SPECTROSCOPY OF HETEROGENEOUS MATERIALS

REQUIRES REPRODUCIBLE PRESSURE CONTROL

ABSTRACT

Attenuated total reflectance Fourier transform infrared spectroscopy (ATR-FTIR), in which the sample is compressed against an internal reflection element, is a popular technique for rapid infrared spectra collection. However, depending on the accessory design, the pressure applied to the sample is not always well controlled. While collecting data from fabrics with heterogeneous coatings, we have observed systematic pressure-dependent changes in spectra that can be eliminated by reproducible pressure control. We describe a pressure sensor adapted to work with an ATR tower to enable more rigorous control of pressure during ATR sampling.

INTRODUCTION

Attenuated total reflectance Fourier transform infrared spectroscopy is a popular technique for qualitative identification of polymeric materials due to its rapid and nondestructive sampling, and sensitivity to chemical and structural variations.[1-4] Forensic research in our research groups have focused on the IR spectroscopy of surfaces of fabrics coated with polymer substrates and blood.[5-12] More generally in forensic applications, ATR-IR has been used to confirm trace fiber identifications, and to detect, identify, and measure amounts of illicit drugs and other trace evidence.[13-15]

In ATR, the sample is compressed against the internal reflective element using a pressure tower. ATR accessories typically have either a lock mechanism to define preset pressures, or a graduated scale indicating qualitative levels of applied pressure, but actual

61

measurement of the pressure is absent in most designs, and repeatability is not guaranteed. However, ATR spectra are sensitive to pressure applied on samples.[2, 16-19] In some cases, the influence of variations in applied pressure cab be eliminated by preprocessing after data collection. Specifically, transforms (such as standard normal variate, SNV, or multiplicative signal correction, MSC) that average and standardize each spectrum in a data set effectively remove variations in spectral baseline and normalize spectra to commensurate scales.[20, 21] However, when polymeric materials have multiple thin layers of different geometries and compositions, pressure differences may change the surface orientation or, by compression, change the effective sampling depth.[2, 22] Pressure may also deform a polymeric material to change its crystallinity, which may alter its spectrum by diminishing or enhancing affected vibrational modes.[16] For fabrics with heterogeneous coatings, variations in applied pressure will directly influence sampling composition and such changes in the spectra cannot be eliminated using preprocessing. Calibration models built on spectra collected without adequate control of pressure, may be biased.

In the present work, we have examined cotton samples with heterogeneous blood coatings to illustrate spectral differences that arises from variations in applied pressures. Our approach in inexpensive and direct: a commercially available pressure sensor is inserted between the sample and pressure tower to monitor pressure during ATR sampling to enable more reproducible data acquisition.

METHOD

Cotton Samples

One 2″ × 2″ red cotton swatch was sonicated for 60 min. in deionized water and suspended to dry for 24 h. After placing the fabric swatch over a small box to suspend the target area, the fabric was lightly coated with 10× dilute rat blood from the upper side using a brush and hung again to dry for 24 h.

Pressure Sensor

A Flexiforce pressure sensor (Sparkfun Electronics, Niwot, CO) was employed to monitor pressure during ATR sampling as shown in Figure 3.1. Glass slides were placed on both sides of the pressure sensor to ensure even distribution of pressure. Electrical resistance of the sensor (inversely proportional to pressure) was measured using a digital multimeter (Goldstar DM9183, Seoul).

Pressure Sensor Calibration

Objects with different weight (5 lbs, 8 lbs, 11 lbs, 15 lbs, 20 lbs, 30 lbs) were measured using a scale. Weighted objects were placed over the tip on the ATR pressure tower. Three replicate readings from the multimeter were recorded for each weight level for calibration.

IR spectra collection

A Thermo Nicolet IS5 Fourier transform infrared (FT-IR) spectrometer with an ID3 attenuated total reflectance (ATR) accessory (Thermo Scientific, Waltham, MA) was employed. A germanium crystal of 7 mm diameter with a 45 ° incident angle was used as the internal reflective element. Samples were placed upside-down (blood-coated side up) on the ATR crystal. The pressure sensor, sandwiched between the glass slides was placed between the fabric sample and the pressure tower. Six pressure levels at electrical resistance values of 150 kΩ, 100 kΩ, 70 kΩ, 30 kΩ, 15 kΩ, 9 kΩ (higher the pressure, lower the electrical resistance) were applied. Three replicate spectra were collected at each pressure setting using 32 scans per collection at 4 cm^{-1} resolution over the wavenumber range of 700 cm^{-1} to 4000 cm^{-1}.

Data Analysis

Spectra collected were imported into The Unscrambler X (CAMO Software AS, Oslo, Norway) for statistical analysis. An 11–point fourth-order Savitzky-Golay polynomial was used to smooth all spectra.[23] Spectra were copied into two identical data sets, each of which was preprocessed with one of two transforms to investigate their efficacy at removing pressure effects. For each spectrum, the standard normal variate (SNV) transform subtracts the mean of the spectral intensities from the spectral intensity at each wavenumber, then divides each centered intensity by the standard deviation of those values. SNV removes multiplicative interferences due to scatter and particle size.[20] The second preprocessing transform tested was the extended multiplicative signal correction, which regresses each spectrum in the data matrix on the mean spectrum of the

64

entire data, then uses the slope and intercept to adjust each spectrum.[24] These steps attempt to correct for additive baseline effects, multiplicative scaling effects, and interference effects.[21]

After preprocessing, the spectra in each data set were mean centered for principal component analysis (PCA) by eigenanalysis of the respective covariance matrices, for comparison of the data sets in a reduced-dimensional space.

RESULTS AND DISCUSSION

A calibration was built to estimate the force applied in the spectra collection. (Figure 3.2) A linear relationship is demonstrated between the force applied and the inverse electrical resistance of the pressure sensor. ATR pressure levels in this work were calculated using the calibration to the unit of the force applied (lbs). Results were shown in Table 3.1.

Smoothed spectra of cotton samples with heterogeneous blood coatings acquired at different ATR pressures are shown in Figure 3.3. Consistency is achieved between replicate spectra at the same pressure level. However, as applied pressure increases (indicated by lower resistance values), the baseline of each spectrum decreases and peak intensities increase. This phenomenon is partially due to the fact that increased pressure compresses the fabric and coating, effectively increasing sampling volume.

Figure 3.4 depicts average spectra collected at different pressures, after smoothing and applying either SNV or EMSC. Comparing Figure 3.4(A) to 3.4(B), EMSC preprocessed spectra exhibit a flatter and more consistent base line than spectra after

65

SNV processing, for which the slope of the baselines for each spectrum are much more inconsistent. In both cases, peak intensity variations due to different sampling volume and baseline offset of spectra were eliminated. However, pressure effects remain in the spectra, seen as intensity differences for peaks appearing in amide A (3300 cm^{-1}), amide B (2800 cm^{-1} to 3000 cm^{-1}), amide I (~1650 cm^{-1}), amide II (~1540 cm^{-1}), and amide III (1200 cm^{-1} to 1350 cm^{-1}) regions.[25-27] These perturbations are due to the pressure-induced effects as a consequence of the heterogeneous blood coating, and cannot be eliminated using either SNV or EMSC preprocessing.

Projections into the space of the first two principal components (PC) are shown in Figure 3.5 for the smoothed spectra preprocessed by SNV or EMSC, and collected at different ATR pressures. In the case of SNV preprocessing (Figure 3.5A), data points representing spectra at different applied pressures are correlated with increasingly positive values with respect to the axis representing the second PC. For EMSC preprocessing, spectra at increasingly higher pressures are ordered, and thus correlated with, increasing pressure from low to high projections along the direction of the first PC. As stated above, base line tilting still exists in the spectra after SNV, which can leads to the fact that instead of the first PC, the second PC contains the variations separates data in Figure 3.5(A).

PC loadings, for spectra preprocessed by SNV and EMSC are shown in Figure 3.6. Loadings express the eigenvector components as correlations with the original spectral variables. Thus, spectral regions correlated with pressure changes include the amide A (3300 cm^{-1}), amide B (2800 cm^{-1}-3000 cm^{-1}), amide I (~1650 cm^{-1}), amide II (~1540 cm^{-1}) regions, as well as the CO_2 peak (2400 cm^{-1}).[25-27] Due to the heterogeneous

66

blood coating, as pressure increases, fabric with a more concentrated coating is compressed in the ATR sampling area, increasing the sampled blood amount. The changes are most prominent in regions of high absorbance, which occur or blood samples at amide peak regions. Similar effects will occur when samples have multiple thin layers of different compositions.

Cotton fabric is porous, and air is trapped within interstitial volumes in the fabric. As sampling pressure increases the air content will squished out. As a result the intensity of the CO_2 peaks decrease as shown in Figure 3.4. The CO_2 peak presence is also seen in the PC loadings (Figure 3.6) as a noticeable spectral variable. This phenomenon indicates that consistency of pressure applied is essential when collecting ATR-FTIR spectra on porous samples.

Score plots for the corresponding second PC (for SNV processed spectra) and the first PC (for EMSC processed spectra), plotted against pressure sensor resistance are shown in Figure 3.7. The variability of the PC scores decreases as applied ATR pressure increases. This observation suggests that higher pressure is preferred for ATR sampling, because it improves spectral reproducibility. However, the hardness of various internal reflective elements (*e.g.*, diamond *vs.* germanium), as well as the physical nature of the sample should be considered when selecting the pressure to be applied.

CONCLUSIONS

Preprocessing methods like SNV and EMSC can reduce or eliminate the spectral variation due to path length changes caused by different applied pressures on samples

67

using ATR-FTIR. However, the spectra of cotton sample with heterogeneous blood coating in this work indicates that different pressure levels applied will vary the effective sampling volume thus composition of sampling content will change. As a result, variations occur at CO_2 and amide peak regions remain noticeable in the spectra after preprocessing. Therefore, pressure control is necessary for more reproducible data acquisition using ATR.

A pressure sensor was introduced in this work to monitor and control pressure applied on samples. Principal component analysis of heterogeneous blood coated cotton samples with different applied pressure demonstrated the accuracy, reproducibility of this technique.

Variation changes of spectra, collected using varied ATR pressures, demonstrated using corresponding PC scores suggests that using a higher possible pressure without damaging the internal reflective elements or deform the sample nature is preferred in real world application.

ACKNOWLDEGEMENTS

REFERENCES

(1) R. A. Merrill , E. G. Bartick. "Analysis of Pressure Sensitive Adhesive Tape: I. Evaluation of Infrared ATR Accessory Advances". *J Forensic. Sci.* **2000**. 45(1): 93–98.

(2) P. Yang, X. Meng, Z. Zhang, B. Jing, J. Yuan, W. Yang. "Thickness Measurement of Nano Scales Polymer Layer on Polymer Substrates by Attenuated Total Reflection Infrared Spectroscopy". *Anal. Chem.* **2005.** 77: 1068-1074.

(3) G. Kleideiter, M. D. Lechner, W. Knoll, "Pressure Dependence of Thickness and Refractive Index of Thin PMMA-films Investigated by Surface Plasmon and Optical Waveguide Spectroscopy". *Macromol. Chem. Phys.* **1999.** 200: 1028-1033.

(4) K. R. Kirov, H. E. Assender. "Quantitative ATR-IR Analysis of Anisotropic Polymer Films: Extraction of Optical Constants". *Macromolecules*. **2004.** 37: 894-904.

(5) H. Brooke, M. R. Baranowski, J. N. McCutcheon, S. L. Morgan, M. L. Myrick. "Multi-mode Imaging in the Thermal Infrared for Chemical Contrast Enhancement. Part 1: Methodology". *Anal. Chem.* **2010.** 82: 8412-8420.

(6) H. Brooke, M. R. Baranowski, J. N. McCutcheon, S. L. Morgan, M. L. Myrick. "Multi-mode Imaging in the Thermal Infrared for Chemical Contrast Enhancement Part 2: Simulation Driven Design". *Anal. Chem.* **2010.** 82: 8421-8426.

69

(7) H. Brooke, M. R. Baranowski, J. N. McCutcheon, S. L. Morgan, M. L. Myrick. "Multi-mode Imaging in the Thermal Infrared for Chemical Contrast Enhancement Part 3: Visualizing Blood on Fabrics". *Anal. Chem.* **2010.** 82: 8427-8431.

(8) M. L. Myrick, M. Simcock, M. R. Baranowski, H. Brooke, S. L. Morgan, J. N. McCutcheon. "The Kubelka-Munk Diffuse Reflectance Formula Revisited". *Appl Spectroscopy Reviews.* **2011.** 46(2): 140-165. 114.

(9) M. R. Baranowski, H. Brooke, J. N. McCutcheon, S. L. Morgan, M. L. Myrick. "Coating Effects on Fabric Infrared Reflectance Spectra". *Appl. Spectrosc.* **2011.** 65(8): 876-884.

(10) M. L. Myrick, S. L. Morgan, "Infrared Specular Reflection Calculated for Polymer Films on Polymer Substrates: Models for the Spectra of Coated Plastics". *Spectrosc.* **2012.** 27: 40-56.

(11) S. A. DeJong, W. L. O'Brien, Z. Lu, B. M. Cassidy, S. L. Morgan, and M. L. Myrick. "Optimization of Gap Derivatives for Measuring Blood Concentration of Fabric from Vibrational Spectroscopy". *Appl. Spectrosc.* **2015.** 69(6): 733-748.

(12) S. A. DeJong, Z. Lu, B. M. Cassidy, W. L. O'Brien, S. L. Morgan, M. L. Myrick. "Detection Limits for Blood on Four Fabric Types Using Infrared Diffuse Reflection Spectroscopy in Mid- and Near-Infrared Spectral Windows". *Anal Chem.* **2015.** DOI: 10.1021/acs.analchem.5b01825.

(13) L. Cho, J. A. Reffner, B. M. Gatewood, D. L. Wetzel. "Single Fiber Analysis by Internal Reflection Infrared Microspectroscopy". *J Forensic Sci.* **2001.** 46(6): 1309–1314.

(14) C. V. Koulis, J. A. Reffner, A. M. Bibby. "Comparison of Transmission and Internal Reflection Infrared Spectra of Cocaine". *J Forensic Sci.* **2001.** 46(4): 822–829.

(15) E. G. Bartick. "Applications of Vibrational Spectroscopy in Criminal Forensic Analysis". Applications in Industry, Materials and the Physical Sciences. **2006.** DOI: 10.1002/0470027320.s7003

(16) F. Friedrich, P.G. Weidler. "Contact Pressure Effects on Vibrational Bands of Kaolinite During Infrared Spectroscopic Measurements in a Diamond Attenuated Total Reflection Cell". *Appl. Spectrosc.* **2010.** 64(5): 500-506.

(17) R. Helmy, G. X. Zhou, Y. W. Chen, L. Crocker, T. Wang, R. M. Wenslow. "Characterization and Quantitation of Aprepitant Drug Substance Polymorphs by Attenuated Total Reflectance Fourier Transform Infrared Spectroscopy A". *Anal. Chem.* **2003.** 75: 605-611.

(18) G. Kleideiter, M. D. Lechner, W. Knoll. "Pressure Dependence of Thickness and Refractive Index of Thin PMMA-Films Investigated by Surface Plasmon and Optical Waveguide Spectroscopy". *Macromol. Chem. Phys.* **1999.** 200: 1028–1033.

(19) G. Kos, H. Lohninger, R. Krska. "Development of a Method for the Determination of Fusarium Fungi on Corn Using Mid-Infrared Spectroscopy with Attenuated Total Reflection and Chemometrics". *Anal. Chem.* **2003.** 75: 1211-1217.

(20) R.J. Barnes, M.S. Dhanoa, S.J. Lister. ''Standard Normal Variate Transformation and De-Trending of Near-Infrared Diffuse Reflectance Spectra''. *Appl. Spectrosc.* **1989.** 43(5): 772-777.

(21) N. K. Afseth, A. Kohler. "Extended Multiplicative Signal Correction in Vibrational Spectroscopy, a Tutorial". *Chemometrics. Intell. Lab.* **2012.** 117: 92-99.

(22) A. Kaito, K. Nakayama. "Surface Orientation in the Sheet of a Liquid Crystalline Poly(ester amide) Characterized by Reflection Infrared Spectroscopy". *Micromoles.* **1992.** 25: 4882-4887.

(23) A. Savitzky, M.J.E. Golay. ''Smoothing and Differentiation of Data by Simplified Least Squares Procedures''. *Anal. Chem.* **1964.** 36(8): 1627-1639.

(24) P. S. Panero, F. S. Panero, J. S. Panero, H. E. B. Silva. "Application of Extended Multiplicative Signal Correction to Short-Wavelength near Infrared Spectra of Moisture in Marzipan". *Journal of Data Analysis and Information Processing.* **2013.** 1: 30-34.

(25) K.M. Elkins. "Rapid Presumptive 'Fingerprinting' of Body Fluids and Materials by ATR FT-IR Spectroscopy", *J. Forensic. Sci.* **2011.** 56: 1580–1587.

(26) S. Cai, B. R. Singh. "Identification of β-turn and Random Coil Amide III Infrared Bands for Secondary Structure Estimation of Proteins". *Biophys. Chem.* **1999.** 80: 7-20.

(27) S. Cai, B. R. Singh. "A Distinct Utility of the Amide III Infrared Band for Secondary Structure Estimation of Aqueous Protein Solutions Using Partial Least Squares Methods". *Biochemistry.* **2004.** 43: 2541-2549.

Table 3.1. Conversion of electrical resistance of the pressure sensor to the force applied.

Electrical Resistance (kΩ)	Force Applied (lbs)
150	6.02
100	8.81
70	12.39
30	29.29
15	56.15
9	93.28
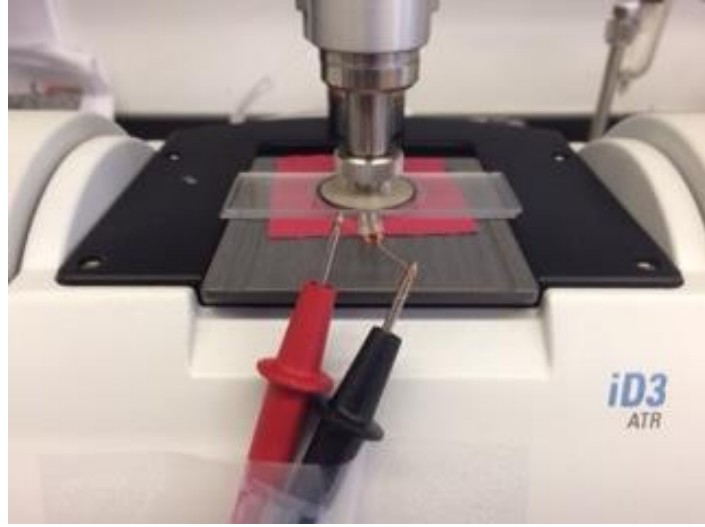
(A)   (B)

Figure 3.1. (A) ATR pressure measurement setup; (B) Close-up of pressure sensor between glass slides and circuit connection to multimeter probes.
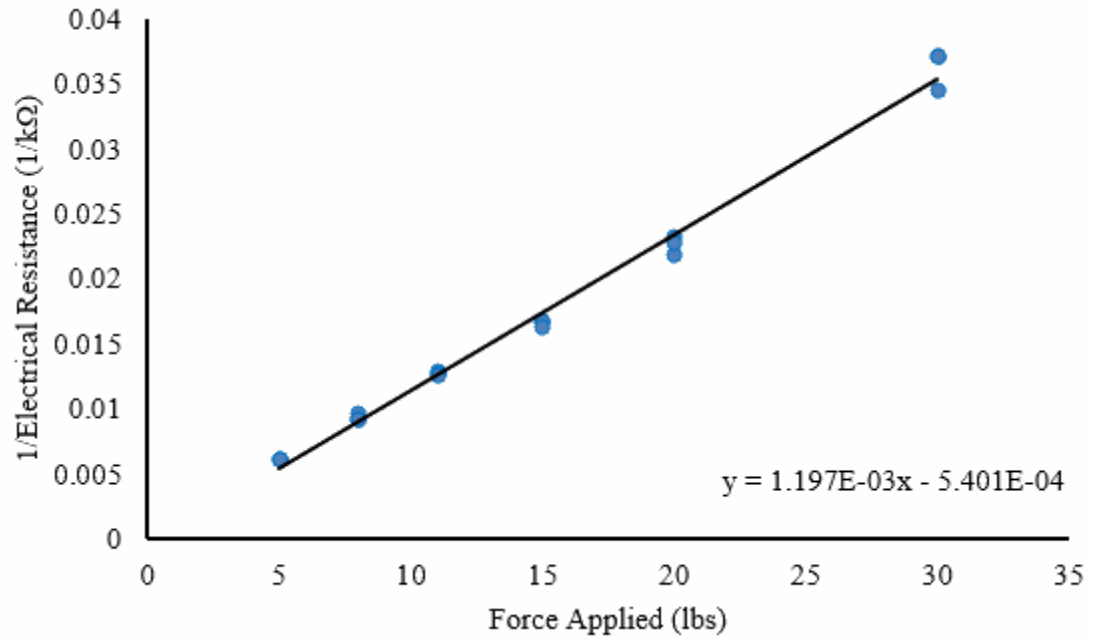
Figure 3.2. Calibration of the force applied *vs.* one over the electrical resistance of the pressure sensor.
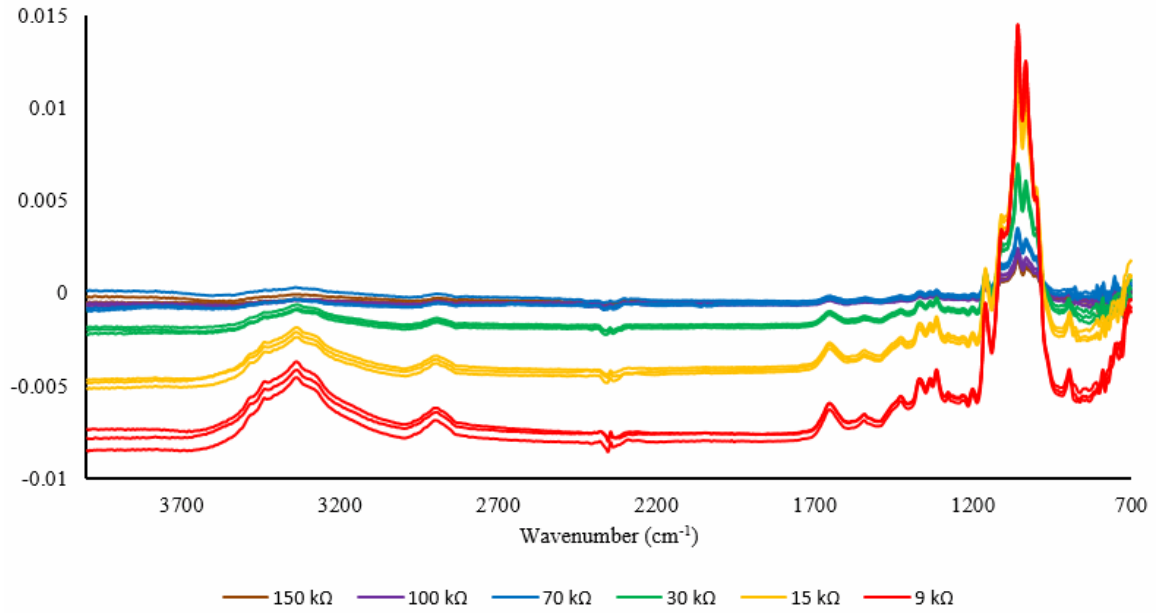
Figure 3.3. Spectra of cotton samples with heterogeneous blood coating collected under different ATR pressures (pressure increases from up to bottom).
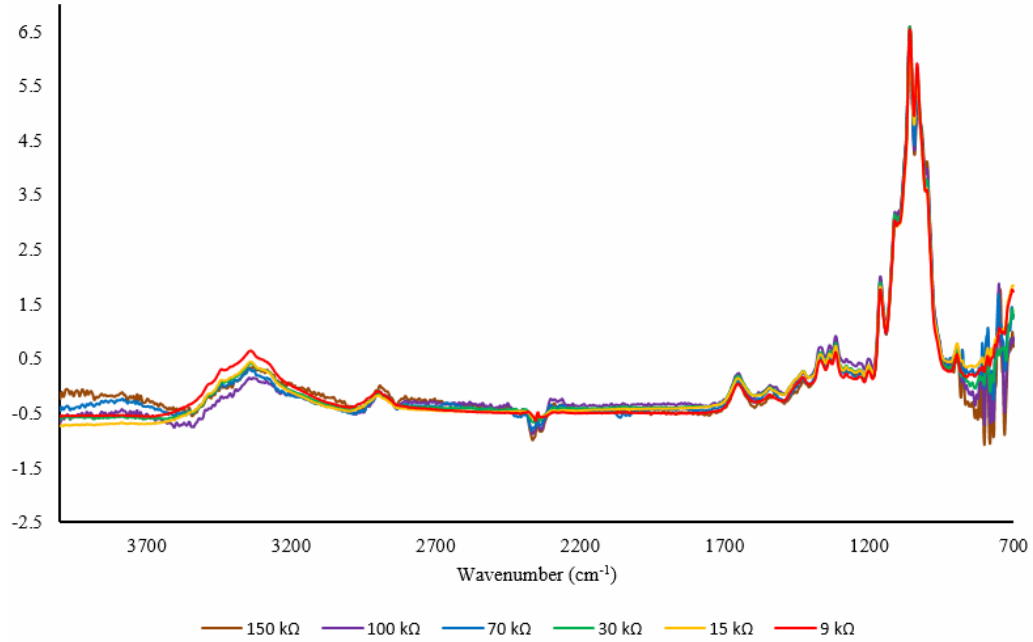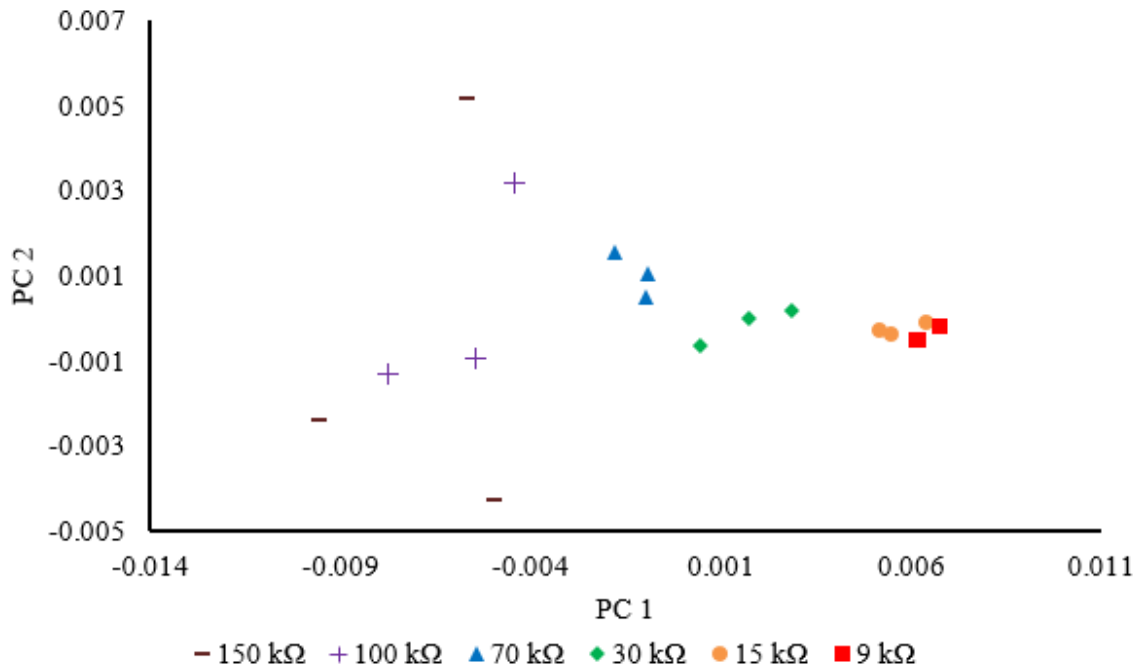
(A)
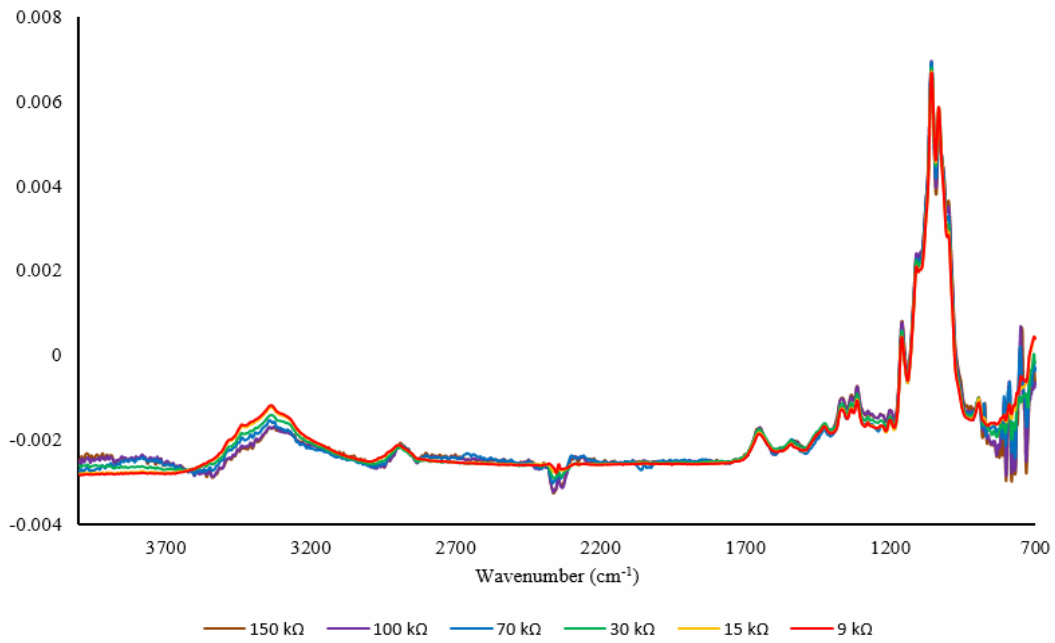
(B)

Figure 3.4. Spectra (after smoothing and preprocessing) acquired at varying ATR pressures: (A) standard normal variate; (B) extended multiplicative signal correction.
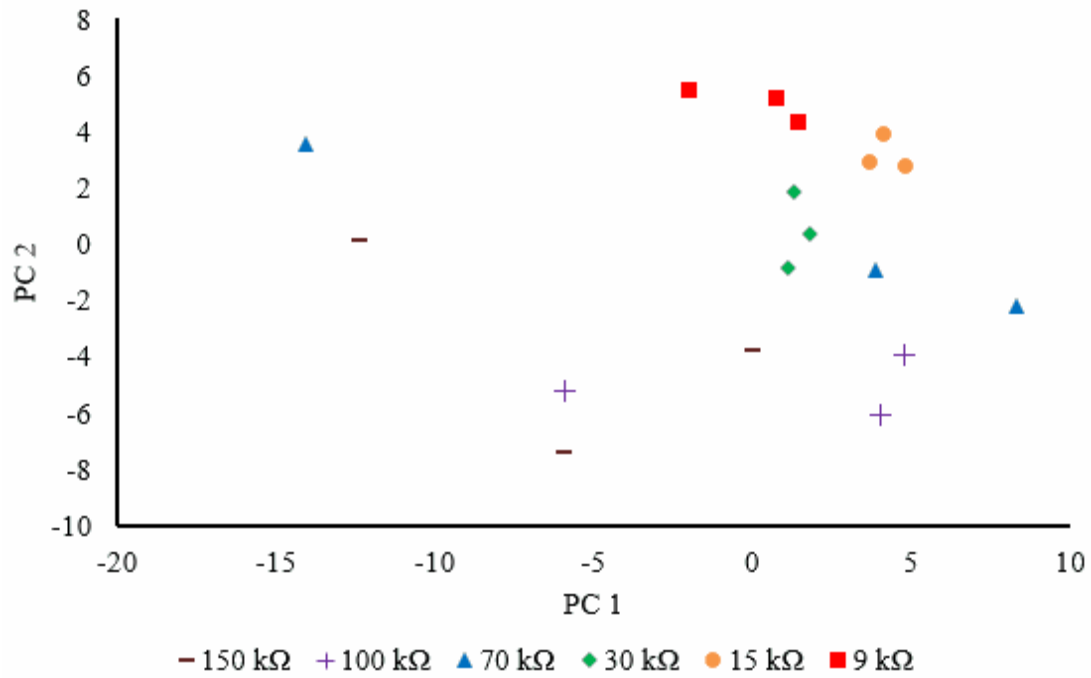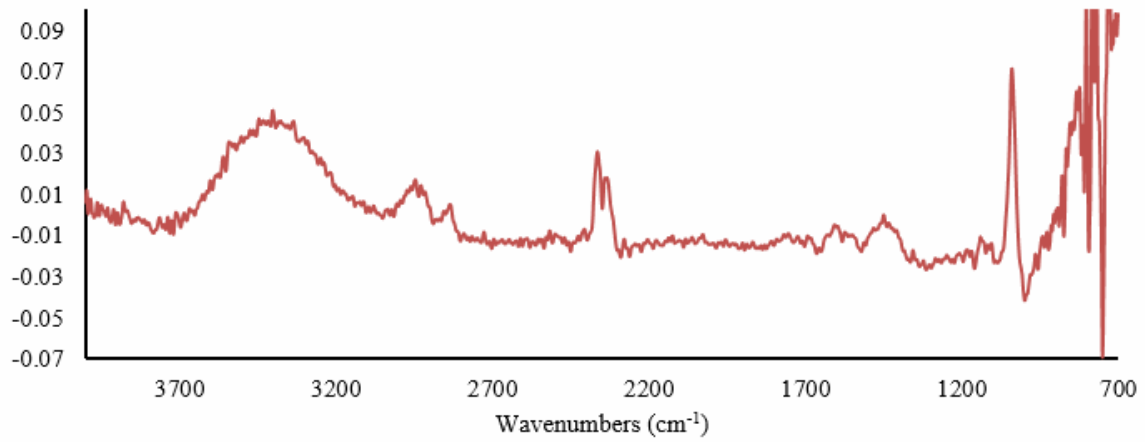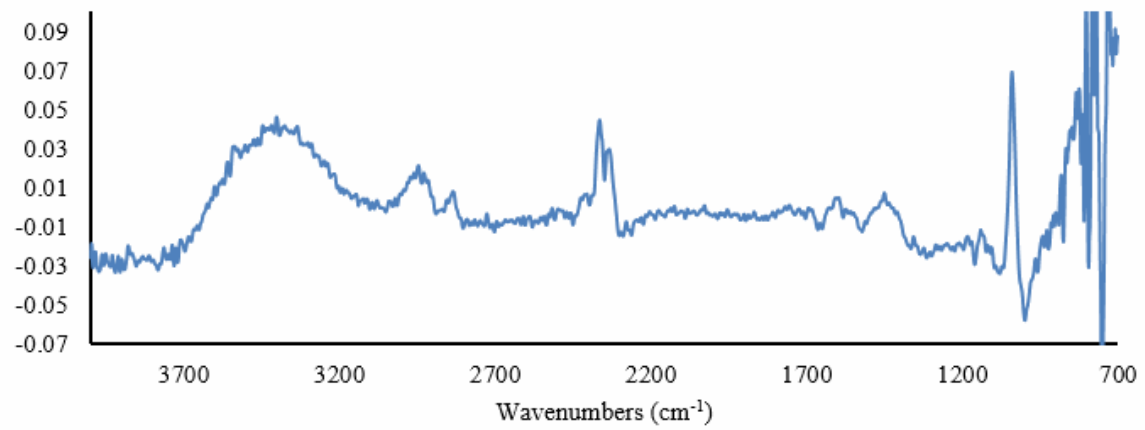
(A)

(B)

Figure 3.5. Principal component projections analysis of smoothed spectra: (A) after SNV preprocessing; (B) after EMSC preprocessing. Color indicates applied ATR pressure.
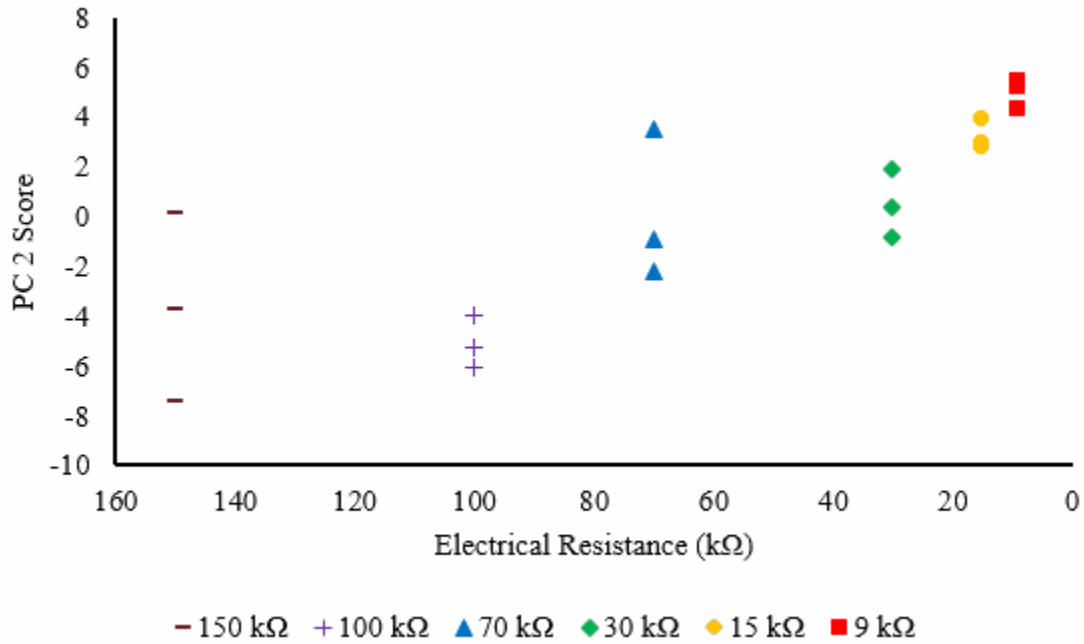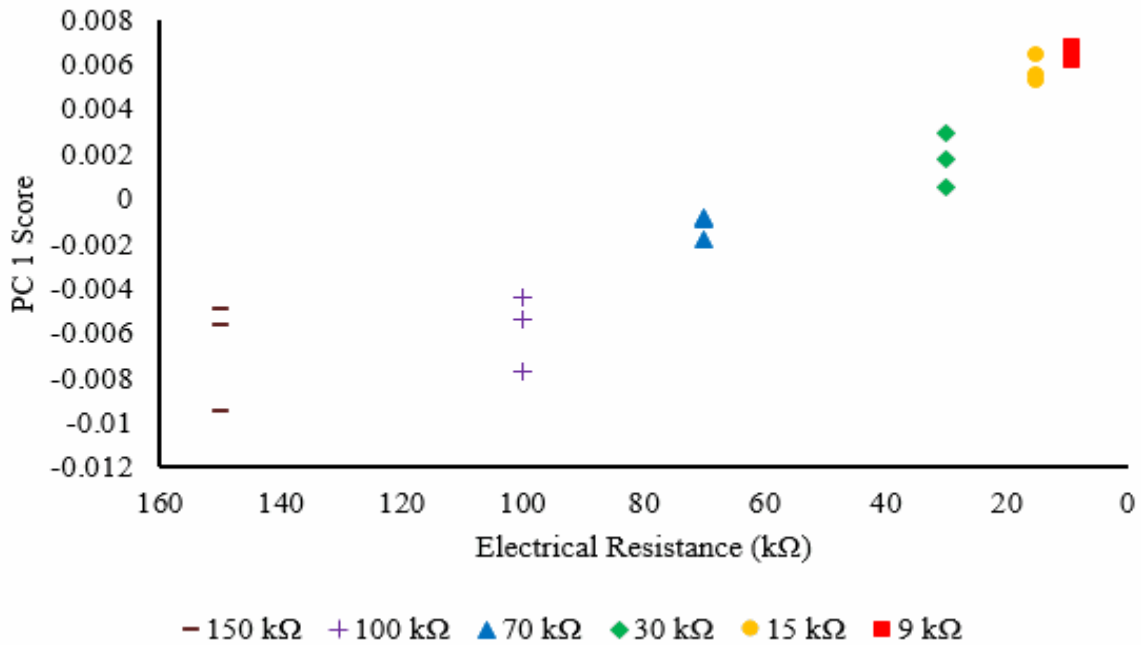
(A)

(B)

Figure 3.6. Loading plots for spectra preprocessed by: (A) SNV (second PC); (B) EMSC (first PC).

(A)

(B)

Figure 3.7. Principal component scores *vs.* electrical capacity of the pressure sensor, which indicates the different pressures applied: (A) SNV transformed data; (B) EMSC transformed data.